ADVANCED MATERIALS INTERFACES
www.advmatinterfaces.de

Bonding-Enhanced Interfacial Thermal Transport: Mechanisms, Materials, and Applications

*Xu-Dong Zhang, Guang Yang, and Bing-Yang Cao**

Rapid advancements in nanotechnologies for energy conversion and transport applications urgently require a further understanding of interfacial thermal transport and enhancement of interfacial thermal conductance (ITC). Sandwiching an intermediate material between two materials has led to a new insight on enhancing electron and phonon transportation, and is enabling the possible regulation of ITC, which has attracted increasing interest over the past decades. Herein, this strategy is named as thermal bonding, following the terminology of mechanical bonding and electrical bonding in microelectronics. The authors systematically summarize the interfacial thermal transport enhanced by thermal bonding from the category of interfacial thermal transport mechanisms, thermal bonding materials (TBMs), related applications, and potential challenges. Especially, the influence factors of interfacial heat transfer are highlighted, from three points, including interaction forces (van der Waals force, hydrogen bond, covalent bond, and metal bond), electron density, and phonon vibration density of states. The authors also outline and classify TBMs into metal bonding materials, organic bonding materials, and inorganic nonmetal bonding materials. As a novel and promising interface science and engineering field, it is believed that thermal bonding strategy will provide scientists and engineers more inspiration to understand interfacial thermal transport and solve the interfacial thermal challenges.

1. Introduction

Interfaces are considered as the devil for heat transfer. The drastic jumps of material microstructures and elemental compositions at the interface severely impede electron and phonon transport and thus lead to a large temperature jump. The first experimental observation of this phenomenon was when Kapitza measured a nonzero temperature difference across a copper/liquid helium interface.[1] With the characteristic length approaching the nanoscale in materials and devices, thermal transport across the interface is currently becoming dominant due to the non-Fourier effect and the large interface density.[2,3] Subsequently, the complexity and importance of interfacial heat transfer have gathered substantial attention.[4–6]

Interfacial heat transfer challenges are ubiquitous in energy conversion and transport processes, such as electronic chips,[7–9] batteries,[10–12] thermal management materials,[13–15] nanotherapies,[16] and nanofluids.[17–19] The chip is manufactured by stacking and etching various materials, which generates hundreds of micro/nano interfaces. Likewise, for the battery, the interface of electrolyte and positive (negative) electrodes will undergo redox chemical reactions, which will significantly affect thermal safety. Thermal interface material (TIM) is a typical thermal management material that is usually used to fill the interface gap. As the TIM thickness decreases, the proportion of interfacial thermal resistance increases (**Figure 1**), which occupies 70% of the contact thermal resistance when the gap equals 10 μm. The interfacial thermal resistance has an even larger proportion for high thermal conductivity TIMs, such as solder. Unfortunately, these interfacial heat transfer bottlenecks ultimately lead to a decrease in material function and reliability. Therefore, enhancing interfacial thermal transport is an imperative scientific and technical challenge faced by many frontiers.

Improving the electron and phonon transmission is the key to enhancing interfacial heat transfer. On an atomic level, different atoms interact through metal bonds, covalent bonds, hydrogen bonds, van der Waals forces, etc. Such interactions will directly affect electron and phonon transmission. Statistics of the kinetic energy of heat carriers thus lead to macroscopic interface heat transfer parameters, such as interfacial thermal resistance or interfacial thermal conductance (ITC). To improve the transmission of the heat carriers, intermediate material is usually inserted into the interface.[25] Indium is the most commonly used intermediate material,[26] and it easily diffuses into other metal materials to form metal bonds, which benefits electron transmission. In addition, sulfide group-modified single alkane molecule (SAM) can form covalent bonds with metals to enhance phonon transmission.[27] Therefore, intermediate materials play a vital role in improving the transport of heat carriers.

Bonding is a common terminology in microelectronic fabrication.[28] Electrical bonding improves the electrical conductivity

X.-D. Zhang, G. Yang, B.-Y. Cao
Key Laboratory for Thermal Science and Power Engineering of Ministry of Education
Department of Engineering Mechanics
Tsinghua University
Beijing 100084, China
E-mail: caoby@mail.tsinghua.edu.cn

The ORCID identification number(s) for the author(s) of this article can be found under https://doi.org/10.1002/admi.202200078.

DOI: 10.1002/admi.202200078

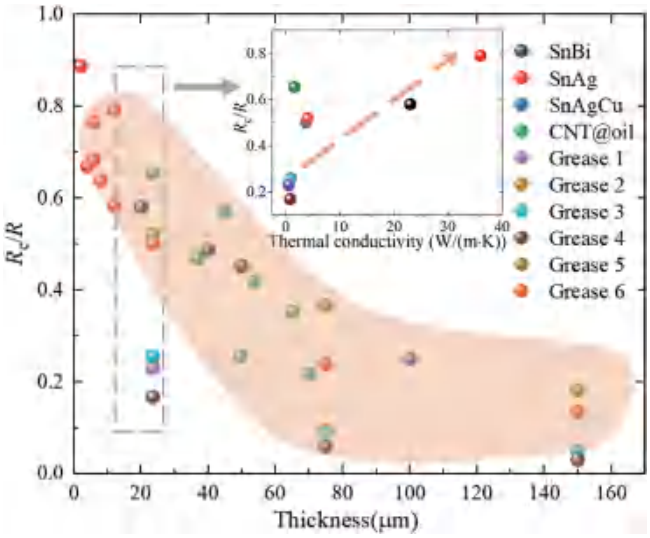

Figure 1. The variation of interfacial thermal resistance with the thickness and thermal conductivity of TIM. R equals the sum of R_c and thermal resistance of TIM, where R is the contact thermal resistance, and R_c is the interfacial thermal resistance. The data was summarized and calculated from refs. [20–24].

of the interface,[29] and mechanical bonding improves the mechanical strength of the interface.[30] Surprisingly, there is no related concept for heat. This article follows this expression and proposes the concept of thermal bonding. Thermal bonding is an interfacial heat transfer method to improve the heat carrier transmission by sandwiching an intermediate material between two materials. The intermediate layer is also called the thermal bonding material (TBM). This review mainly covers the thermal bonding field in terms of the heat transfer mechanism, influence factors, TBMs, and applications, as shown in **Figure 2**.

In this review, interfacial bonding heat transfer is discussed using the following stepwise approach: 1) the electron and phonon transmission models, and microscale interfacial heat transfer mechanisms for metal/metal, metal/nonmetal, nonmetal/nonmetal, are generally introduced. 2) The effects of the four bonding forces, electron density, and phonon vibration density of states on heat transfer are thoroughly discussed. 3) The TBMs to enlarge ITC are summarized. 4) The applications of thermal bonding strategy are highlighted. 5) Finally, to wrap up this review, the conclusion and perspectives are stated. The insights and summarized advances of this review are useful for understanding interfacial thermal transport and dealing with interfacial thermal challenges.

2. Interfacial Heat Transfer Mechanism

It's intelligible to elucidate the microscopic mechanism of interfacial heat conduction by considering the process between the initial state of energy input and the final state of establishment of steady energy balance. For interfaces composed of different materials or different phases of the same material, the energy states of heat carriers (electron energy band, phonon dispersion, etc.) of each side are different. At the beginning of energy being input from heat sources on one side (hot side), heat transfers from this side to the other (cold side) across the interface, while the transmission of some modes of heat carriers is restricted because of mismatch of energy states. At this moment, the heat flux across the interface is less than the total energy input by heat sources, implying an unsteady state. To

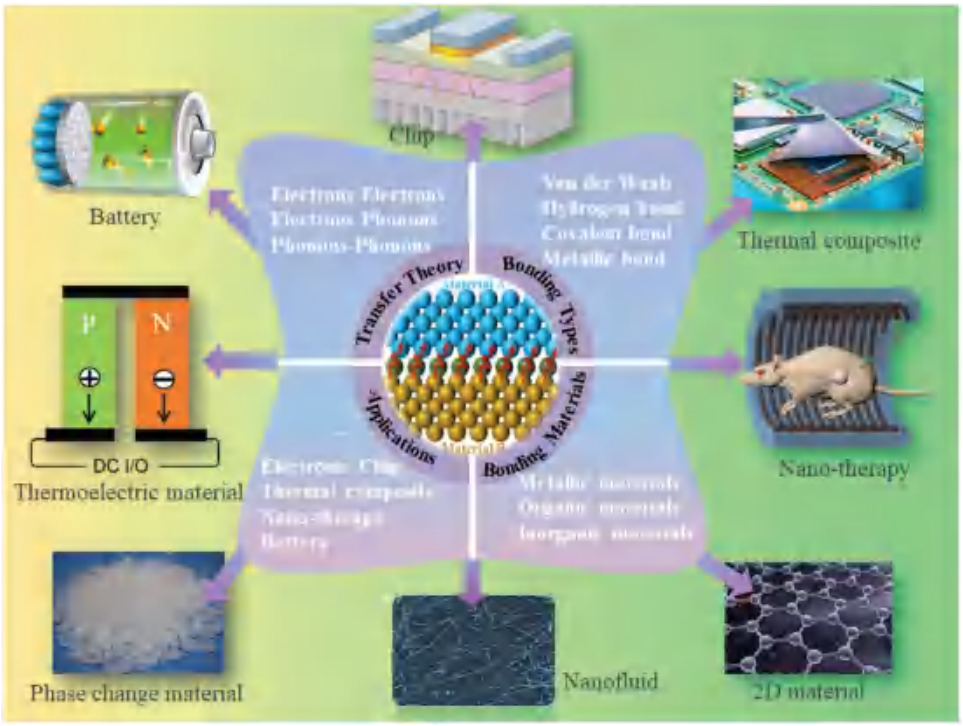

Figure 2. The connotation of thermal bonding.

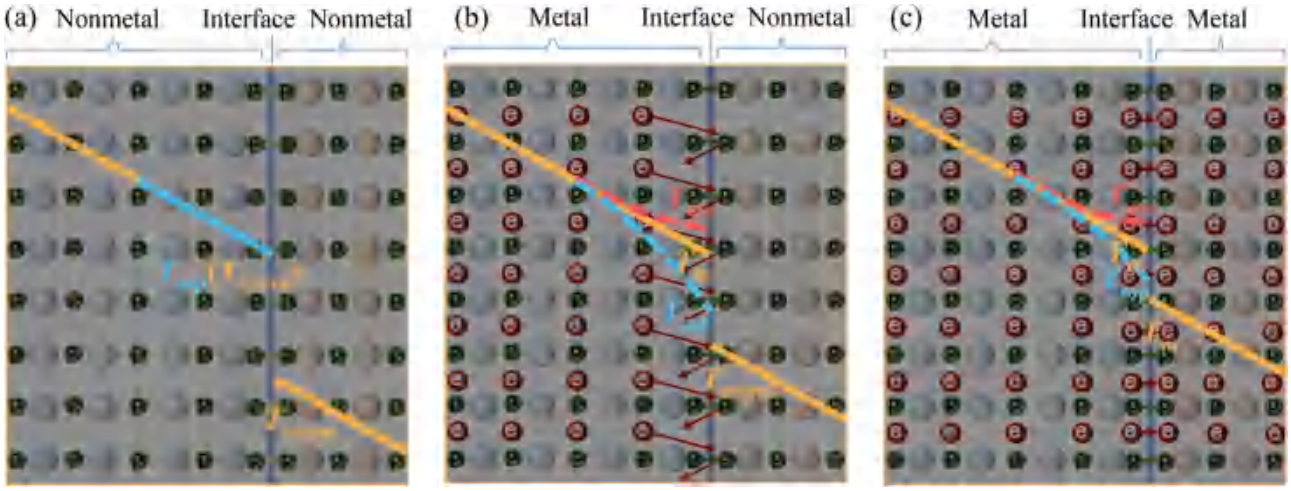

Figure 3. Schematic of heat carrier transmission. a) Nonmetal/nonmetal interface; b) Metal/nonmetal interface; c) Metal/metal interface.

complement the heat flux and reach energy balance finally, the carrier occupation numbers on each allowable energy level of hot side will increase consistently to open additional heat channels, exhibiting a macroscopic temperature rise of hot side as well as a distinct temperature jump at the interface. It is worth mentioning that the interfaces discussed here are perfect plane contacts, though the uneven contacts caused by roughness and imperfection sometimes play a more dominant role, which is not the focus of this review and has been discussed systematically elsewhere.[31]

Heat in solids is mostly carried by electrons or phonons (atomic vibration). According to different types of heat carriers, the interface can generally be divided into nonmetal/nonmetal, metal/nonmetal, and metal/metal interfaces, as shown in **Figure 3**. For the nonmetal/nonmetal interface, the phonon is the dominant carrier. For the metal/metal interface, electrons are the main heat carriers, since the electron-dominated scattering processes at interfaces occur much faster (with time scales in the 10s of picoseconds for metal/metal interfaces) than the phonon-dominated scattering processes across interfaces, which takes place in the several hundred picoseconds to nanosecond time scales.[1] For the metal/nonmetal interface, both electrons and phonons participate in heat conduction, and the interface heat conductance can be regarded as the parallel thermal resistance network, consisting of the energy transmission between electrons in the metal and phonons in the nonmetal (interface electron–phonon coupling), in line with the energy exchange between phonons in both metal and nonmetal. Generally, the thermal transport of metal/metal interface is better than that of metal/nonmetal and nonmetal/nonmetal interface, whose ITC can be greater than an order of magnitude as compared to the typical phonon-dominated conductance. In addition, because phonon transport is affected by the detailed matching characteristics of the phonon dispersion and the strengths of interface forces, it is difficult to compare the ITC of metal/nonmetal and nonmetal/nonmetal directly.

The capacity of interfacial heat transfer is quantified by the ITC, G, which relates the heat flux to the temperature drop at the interface. ITC is also called thermal boundary conductance (TBC), which is inversely related to interfacial thermal resistance R (also called thermal boundary resistance [TBR]). G can be estimated by the following empirical models or computational simulation methods.

2.1. Nonmetal/Nonmetal Interface

In terms of empirical models, nonmetal/nonmetal interfacial heat transfer is classically described by the acoustic mismatch model (AMM) and diffuse mismatch model (DMM),[32–34] and both models are based on harmonicity assumption. In the AMM model, the estimated interface phonon transmittance and interface thermal resistance are given by analogy with the specular refraction and reflection waves at the interface. However, the above assumptions can be satisfied only when the long wavelength phonons dominate the heat conduction because the short wavelength phonons will have significant diffuse scattering at the interface. Therefore, the AMM model can give the estimated interface thermal resistance in accordance with the experimental observations only at very low temperatures (<10 K) and only when low-frequency longwave phonons are dominant. For high temperatures, high-frequency shortwave phonons dominate heat transport, and phonons diffuse significantly at the nonideal interfaces (dense lattice defects, atomic mixing). To explain the phonon diffuse scattering process, Swartz et al. proposed the DMM model.[32] The DMM model is based on two main assumptions: first, the phonon transmittance is isotropic, that is, the transmittance is independent of the phonon incident angle; Second, phonons will lose all memory after diffuse scattering at the interface, that is, photons will be emitted from the interface to both sides according to probability according to VDOS of materials on both sides at the interface.[35] Although the prediction of DMM model is better than that of AMM model near room temperature, the research of Stevens et al.[36] shows that the prediction results of DMM model are still at least one order of magnitude different from the experimental values. In order to overcome the limitation of harmonicity assumption used in both classical AMM and DMM models, Hopkins et al.[37] proposed anharmonic inelastic model to move beyond the harmonic two-phonon scattering assumptions, and

account for energy transmission among three or more phonons at interface. However, all the foregoing models do not take the atomistic nature at the interface into account, which is one of the main flaws of these empirical models.

As for computational simulation methods, atomistic Green's function (AGF) and molecular dynamics (MD) are most extensively used. The AGF approach is based on a system of classical harmonic Newtonian equations with solutions that are in the form of plane waves. From the calculated Green's function matrix, it becomes possible to calculate the mode-dependent interface transmission coefficients for various types of interfaces.[38–41] Nevertheless, the AGF method is usually carried out in the harmonicity approximation. As such, AGF is mainly suitable for low temperatures where anharmonicity has a negligible contribution to thermal transport. In order to accurately quantify the anharmonic thermal transport across the interfaces as well, Dai et al.[42] and Guo et al.[43] have included the three-phonon scatterings in their AGF calculations with the inputs from first-principles simulations. Unlike the AGF approach, MD simulation does not require a priori understanding of heat transport. Furthermore, MD simulation has an anharmonicity inherently based on the assumed potential and therefore includes multiple phonon interactions, rendering it a useful tool to study TBC across various types of material systems. The interfacial thermal transport has been comprehensively studied via either the equilibrium MD (EMD) simulations with the Green–Kubo approach[44] or the nonequilibrium MD (NEMD) simulations by applying heat baths on a computational domain and determining the temperature drop at the interface.[45] In the frame of EMD, Gordiz and Henry[46] calculated the anharmonic interfacial phonon scattering by using the total ITC minus the contribution of harmonic phonon scattering.[47] In terms of NEMD, Kimmo et al.[48] considered both the harmonic transport and first-order anharmonic phonon scattering effects on the ITC. Zhou and Hu[49] later extend the ITC to include both the harmonic process and three-phonon scatterings.

2.2. Metal/Metal Interface

The ITC is usually calculated according to the Wiedemann–Franz law,[50–52] which is that thermal conductance equals the product of electrical conductance, temperature, and Lorentz constant. For metal materials, free electrons are more effective carriers than phonons. Therefore, near room temperature, the thermal conductance contributed by phonons is ignored, and the thermal conductance of electrons calculated by the Wiedemann–Franz law almost equals the total ITC.

2.3. Metal/Nonmetal Interface

There exist three types of heat carrier interactions, including electron–phonon coupling in metal, electron–phonon coupling at interface, and phonon–phonon interaction at interface.[53–57] Li et al.[58] established the thermal resistance network of ITC, including electron thermal conductance, phonon thermal conductance, boundary electron–phonon coupling thermal conductance, and boundary phonon–phonon interaction thermal conductance. For the Pb/diamond interface, the ITC is mainly determined by interfacial electron–phonon coupling; for the Ti/diamond interface, the ITC is determined by interfacial electron–phonon coupling and phonon–phonon interaction; for the tin/MgO interface, the thermal conductance is determined by the phonon interaction at the interface. In the work of Sadasivam et al.,[59] the time-domain thermoreflectance (TDTR) results of $CoSi_2$/Si interfaces only agree well with simulation predictions that include all transport processes: elastic and inelastic phonon scattering, electron–phonon coupling in the metal, and electron–phonon coupling across the interface. However, some investigations[60–62] have proven that the elastic phonon transport dominates the thermal transport of epitaxial metal/sapphire interface, and other mechanisms play negligible roles. And the coupling of electrons in Bi and Pb[63] to phonons in diamond substrate does not contribute significantly to the interfacial thermal transport. Moreover, if the metal is a magnetic material, then the phonon–magnon coupling at the interface should be also included.[64]

3. Influence Factors

For a perfectly smooth interface, interaction forces exist between atoms or molecules. From a microscopic scale, increasing the interaction potential between the atoms/molecules is more conducive to electron and phonon transfer. In addition, the electron density and phonon VDOS matching characteristics of the two materials will also affect heat transfer across interface. The larger the overlap of the VDOS of the two materials is, the higher the phonon transmission efficiency. This section will introduce the influence factors of interfacial thermal transport, including bonding forces, electron density, and phonon VDOS matching characteristics.

3.1. Bonding Forces

The bonding forces can be divided into van der Waals force, hydrogen bond, covalent bond, and metal bond. Van der Waals force is an intermolecular interaction force, the hydrogen bond is intermolecular or intramolecular force, the covalent bond is intramolecular force, and the metal bond is atomic force. The forces from small to large are van der Waals force, hydrogen bond, covalent bond, and metal bond. Taking the interfaces of Au/multiple materials as examples, **Figure 4** shows that ITC increases with bonding strength increasing.[65–71] These four forces will be introduced in detail below. **Table 1** listed some experimental values of ITC. What needs to be mentioned here is that the interface bonding strength has the following three expression methods, which are J m^{-2}, mN, and kcal mol^{-1}, and the expression forms used by different researchers are different.

3.1.1. Van der Waals Force

Van der Waals force widely exists at various micro/nano interfaces.[78] When two materials are in contact, van der Waals force usually occurs, such as carbon-based materials/organic

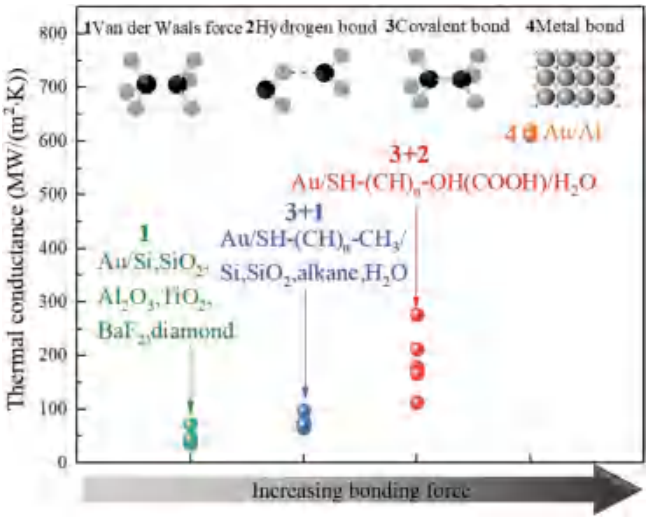

Figure 4. The interfacial thermal conductance between Au and multiple materials.[65–71]

materials, metals/inorganic materials, and metals/organic materials. The AMM model only considered the interface as a very strong interaction and ignored the influence of the interface forces on phonon transmission. The modified AMM has been developed to describe interface phonon transport considering the weak interaction of van der Waals force.[79] **Figure 5**a shows the relationship between interface adhesion energy and phonon transmission coefficient. The horizontal coordinate is interface adhesion energy γ, and the ordinate is modified AMM phonon transfer coefficient/AMM phonon transfer coefficient. When γ approaches 1000 mJ m^{-3}, the ratio is closer to 1; for small γ, the ratio is proportional to γ^2; for minima γ, the ratio is proportional to γ. Figure 5b summarizes the variation of ITC with bonding strength at the interface of metal/inorganic nonmetal.[80,81] The ITC increases with the interfacial bonding strength increasing. The interfacial bonding strength between chromium and inorganic nonmetal solids is the largest, and thus the ITC is largest, followed by aluminum and gold.

The metal/dielectric interfaces widely exist in complementary metal-oxide semiconductor transistors,[84] in form of van der Waals force. In the work of Shi et al.,[85] the ITCs at different metal/β-Ga_2O_3 interfaces were measured by TDTR. The experimental results were 31.2, 17.4, 82.7, and 81.7 MW m^{-2} K^{-1} for Au/β-Ga_2O_3, Ti/β-Ga_2O_3, Ni/β-Ga_2O_3, and Al/β-Ga_2O_3, respectively. Cheng et al.[86] measured the van der Waals bonded Ga_2O_3/diamond interface by TDTR, the ITC was 17 MW m^{-2} K^{-1}. It can be roughly concluded that ITC bonded by van der Waals force is usually small than 100 MW m^{-2} K^{-1}. And the ITCs of Ga_2O_3/SiC range from 20 to 100 MW m^{-2} K^{-1}.[87–89]

Zheng et al.[90] prepared polystyrene thin films/sapphire samples and evaluated the relationship of interface bonding strength and rotation speed in the spin-coating process. With increasing spin-coating speed, the interfacial bonding strength increases gradually, and the ITC increases. The ITC between polystyrene and copper can be increased three times with the spin-coating speed from 2000 to 8000 rmp.

Table 1. Summary of interfacial thermal conductance values measured by experiments.

Bonding material	Interface	Bonding type	Thermal conductance (MW m^{-2} K^{-1})	Measurement method
none	spun-cast PMMA/Si	van der Waals force	9–100	TDTR[72]
none	brush PMMA/Si	van der Waals force	3–40	TDTR[72]
none	Pt/water	van der Waals force	130	TA[73]
none	CNT/octane	van der Waals force	12	TA[74]
none	Au/hexadecane	van der Waals force	28	TTR[75]
none	Au/paraffin wax	van der Waals force	25	TTR[75]
none	Au/Al_2O_3	van der Waals force	45	TTR[68]
none	Au/diamond	van der Waals force	46	TTR[68]
Cl-SAM	Al/H_2O	van der Waals force	60	TDTR[76]
CH_3-SAM	Au/H_2O	van der Waals force	50	TDTR[76]
CH_3-SAM	Au/quartz	van der Waals force	36	TDTR[65]
OH-SAM	Al/H_2O	hydrogen bond + van der Waals	180	TDTR[76]
OH-SAM	Au/H_2O	hydrogen bond + van der Waals	100	TDTR[76]
NH_2-SAM	Au/H_2O	hydrogen bond + van der Waals	130–450	TA[77]
SH-SAM	Cu/silica	covalent bond + van der Waals	430	TDTR[66]
SH-SAM	Au/TiO_2	covalent bond + van der Waals	130	TDTR[66]
SH-SAM	Au/hexadecane	covalent bond + van der Waals	169	TTR[75]
SH-SAM	Au/paraffin wax	covalent bond + van der Waals	165	TTR[75]
SH-SAM	Au/quartz	covalent bond + van der Waals	68	TDTR[65]
none	Al/Cu	metal bond	3700	TDTR[70]
none	Pd/Ir	metal bond	14 000	TDTR[51]

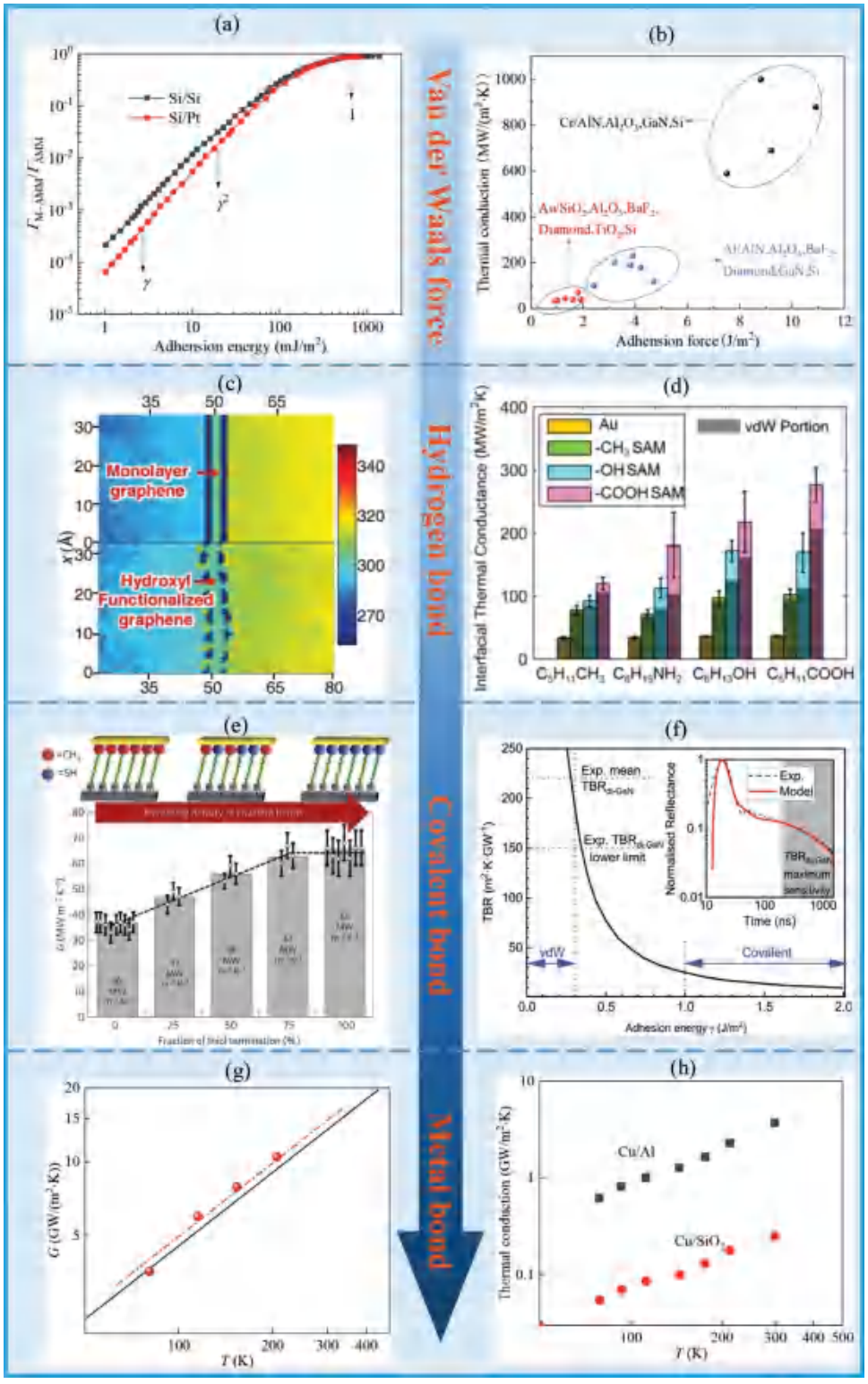

Figure 5. Four types of bonding forces. a) Relationship between adhesion energy and phonon transfer coefficient of modified AMM model. Reproduced with permission.[79] Copyright 2009, American Institute of Physics. b) Relationship between interfacial thermal conductance and interfacial strength between metal/inorganic nonmetal.[80,81] c) Temperature distribution of graphene/PMMA interface modified by hydrogen bond. Reproduced with permission.[82] Copyright 2016, Wiley-VCH. d) ITC of Au/organic liquid modified by hydrogen bond. Reproduced with permission.[69] Copyright 2016, American Chemical Society. e) ITC of Au/SiO_2 using methyl alkanes and mercaptan alkanes as intermediate layers. Reproduced with permission.[65] Copyright 2012, Springer Nature. f) Relationship between ITC and interfacial bonding strength of GaN/diamond predicted by weak bond AMM model. Reproduced under the terms of the CC-BY 4.0 license.[83] Copyright 2021, The Authors, published by IOP Publishing. g) ITC variation of Pd/Ir with

3.1.2. Hydrogen Bond

Hydrogen bond is stronger than van der Waals interaction, and mainly exists in water and organic materials. Hydroxyl (—OH)- or carboxyl (—COOH)-modified single alkane molecules can form hydrogen bonds with water. Harikrishna et al.[91] compared the ITC of gold/water interfaces with different SAMs (CH_3-SAM, ester-SAM, pyrrolyl-SAM, OH-SAM, and COOH-SAM) as bonding layers. OH-SAM and COOH-SAM have maximum ITC, which are two times higher than that of ω–CH_3 modified.

By changing the degree of functionalization, the ITC can be adjusted over a wide range. MD simulations have proven that hydrogen bonding can make organic molecules closer to the interface, increase the interface binding energy, and significantly promote interfacial heat transfer.[69] The detailed analysis of molecular-level details shows that this effective heat transfer comes from the synergistic effect of the electrostatic part and van der Waals part of hydrogen bond (Figure 5d). Zhang et al.[82] established the effective heat transfer path at the graphene/polymethylmethacrylate (PMMA) interface by introducing hydrogen-bonded hydroxyl group at the interface between graphene and PMMA, which can improve the ITC by 273% (Figure 5c).

3.1.3. Covalent Bond

A covalent bond can form at metal/organic, organic/organic, and inorganic/inorganic interfaces. Such a bond is a relatively stable chemical structure in which two or more atoms share their electrons to reach electron saturation. Losego et al.[65] compared the ITC of the Au/quartz interface using CH_3-SAM and SH-SAM as bonding layers, and found that the heat transfer enhancement of SH-SAM was better than that of CH_3-SAM, as shown in Figure 5e. This is because the covalent bond is formed between SH-SAM and Au, while CH_3-SAM and Au interact with van der Waals force. The same observation was drawn at the Cu/SiO_2 interface.[66]

Covalent bond can also be formed at semiconductor material interface.[92] William et al.[83] proposed a weak bond AMM model for predicting the quantitative relationship between the interfacial bonding strength and thermal boundary resistance. On this basis, the effect of interface bonding strength on the thermal resistance of GaN/diamond interface is analyzed by using this model. The results show that the increase of interface bonding strength will significantly reduce the thermal boundary resistance, and the thermal resistance of GaN/diamond interface connected by the covalent bond is less than 1/7 of that under van der Waals force (Figure 5f).

3.1.4. Metal Bond

For the metal/metal interface, when the interface gap is close enough, a metal bond can be formed. The metal bond is formed by the electrostatic attraction between free electrons and metal ions arranged in a lattice. The strength of metal bond is usually inversely related to the metal ion radius and positively related to the free electron density in the metal. The experimental results have proven that the ITC of metal/metal can be calculated by Wiedemann–Franz law, which is that the ITC is proportional to electrical conductance (Figure 5g).[51]

Gundrum et al.[70] measured the thermal conductance of the Al/Cu interface, which is ≈4 GW m^{-2} K^{-1} at room temperature, which is an order of magnitude higher than that of a typical metal–nonmetal interface (Figure 5h). A metal bond is formed between Al and Cu, and the scale of the ITC is GW m^{-2} K^{-1}, while the magnitude of the ITC dominated by covalent bonds, hydrogen bonds, and van der Waals forces is ≈100 MW m^{-2} K^{-1}. Therefore, the metal bond can obtain a large ITC. In addition, Zheng and Jagannadham[93] also experimentally tested the ITC between Cu and various metal films, respectively, and the results were Cu/Al = 7.4 GW m^{-2} K^{-1}, Cu/Au = 4.4 GW m^{-2} K^{-1}, Cu/Sn = 6.7 GW m^{-2} K^{-1}, Cu/Zn = 5.2 GW m^{-2} K^{-1}, and Cu/In = 6.2 GW m^{-2} K^{-1}. The ITC of Cu/Al_2O_3 is only about 100 MW m^{-2} K^{-1}.

3.2. Phonon Vibration Density of States and Electrons Density

From the above analysis, the greater the bonding strength is, the greater the interface thermal conductance. However, an intriguing experiment[94] overturns such positive correlation. For the copper/diamond interface, CH_3-SAM bonding layer (van der Waals force) can obtain a larger interface thermal conductance than the SH-SAM bonding layer (covalent bond). This is because the VDOS of copper is mostly located in the low-frequency region, while that of diamond is located in the high-frequency region, resulting in a small number of phonon transmission channels between these two materials, as shown in **Figure 6**a. Because the VDOS of CH_3-SAM with copper and diamond has more overlap than that of SH-SAM, CH_3-SAM has a better heat transfer enhancement capacity. This experimental result revealed the importance of VDOS overlap. Taking the gold/toluene interface as an example,[27] using SC_{12} as the bonding material, the ITC increased from 13.8 to 67.4 MW m^{-2} K^{-1}, as shown in Figure 6b. The numerical simulation method was used to analyze the overlap of VDOS of the three materials. It found that the VDOS of toluene and SC_{12} have a greater overlap, so there are more phonon transmission channels. Therefore, by introducing intermediate materials to increase the overlap degree of VDOS curves, the interfacial heat transfer can also be improved.

However, if electrons dominate the interfacial thermal transport, the use of a nonconductive bonding layer will hinder electron transport and reduce the interface thermal conductance. An experimental comparison[95,96] has proven that the ITC of covalently bonded Au/SC_nS/GaAs (25.6–28.2 MW m^{-2} K^{-1}) is lower than that of Au/GaAs

temperature, the black dot is the experimental data, the dotted line is the predicted value of Wiedemann–Franz law, and the solid line is the predicted value of electronic DMM model. Reproduced with permission.[51] Copyright 2012, American Physical Society. h) ITC variation of Al/Cu and Cu/Al_2O_3 with temperature. Reproduced with permission.[70] Copyright 2005, American Physical Society.

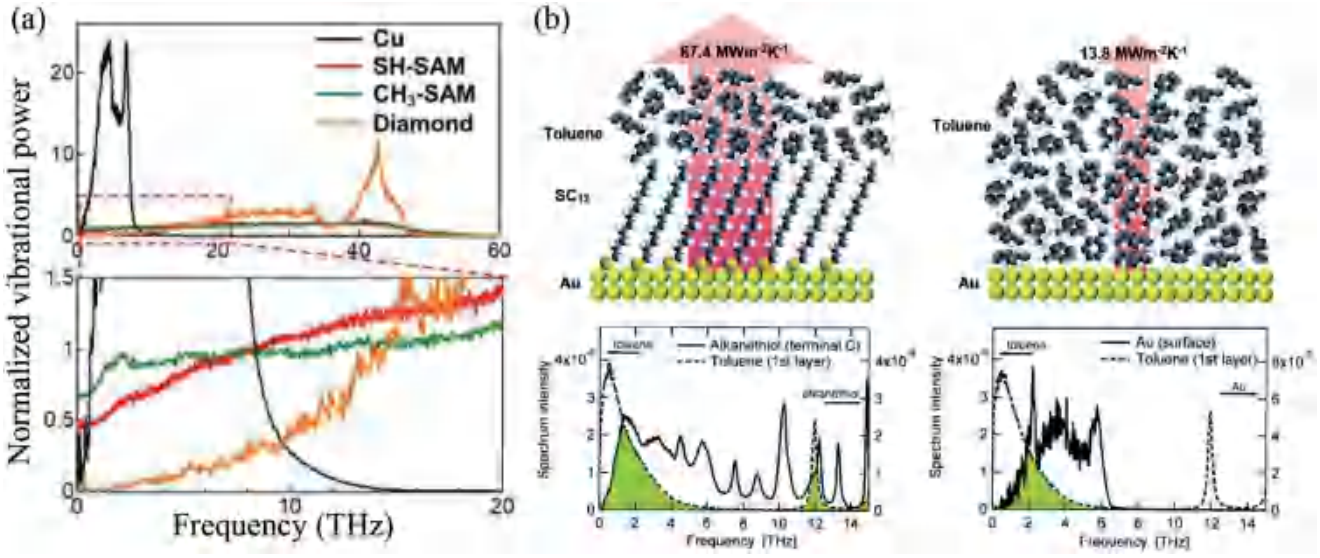

Figure 6. a) Phonon VDOS at Cu/diamond interface. Reproduced with permission.[94] Copyright 2021, American Association for the Advancement of Science. b) Thermal conductance and VDOS at the Au/toluene interface. Reproduced with permission.[27] Copyright 2020, Royal Society of Chemistry.

without bonding layer (180 MW m^{-2} K^{-1}). The electron determines the heat transfer of metal, while the atomic vibration contributes to the majority of the heat transfer of dielectric materials. Therefore, the mismatching of heat carriers caused a worse thermal conductance. This illustrates the importance of the electron density of the bonding material to the interface thermal transport.

4. Thermal Bonding Material

The selection of TBMs is the key to enhancing interfacial heat transfer. The first selection standard is the appropriate electron/phonon transmission characteristics of TBM with upper and lower materials. For the interfaces where electron transmission is dominant, electron-rich materials are preferred; for interfaces where the phonon transmission is dominant, the priorities are bonding materials with a large overlap of VDOS. Second, consider the interfacial bonding strength. The greater the interfacial bonding strength, the larger ITC is. The formation of metal bonds or covalent bonds should be given priority, followed by hydrogen bonds and van der Waals forces.

According to different types of heat carriers and interfacial bonding methods, TBMs can be divided into metal TBMs, organic TBMs, and inorganic nonmetal TBMs, as listed in **Table 2**. The heat carriers of metal TBMs are mainly electrons, which are used to bond the metal/metal interface, and connected to the upper and lower surfaces by metal bonds. The heat carriers of organic TBMs are phonons, which are used to bond the metal/inorganic material interface, the inorganic material/inorganic material interface, the organic material/inorganic material interface, etc., and the upper and lower surfaces are mainly connected by covalent bond, or hydrogen bond, and van der Waals force. The heat carriers of inorganic nonmetal TBMs are phonons, mainly carbon-based materials and semiconductors, which are connected to the upper and lower surfaces by a covalent bond or van der Waals forces. Three types of TBMs are introduced below.

4.1. Metal Thermal Bonding Material

Metal TBMs can be used for metal/metal interface to enhance electron transmission. Solder is required to connect the chip and the substrate, which will generate plenty of metal/metal interfaces.[105] For the metal/metal connection, the first consideration is the mechanical properties and electrical properties, and good thermal properties are pursued on this basis. Therefore, solder is what we call metal TBMs, such as indium, Bi–Zn alloy, Bi–Ag alloy, and Sn–Al alloy (**Figure 7**b). Because the interface generated by soldering process will cause some voids and irregularity,[98] the interface is not a perfect surface, and the ITC is far lower than that in Section 3.1.4. Radebaugh[97] measured the ITC of Cu/In/Cu and Be/In/Cu from 2 to 130 K. With increasing temperature, the ITC first increases and then decreases, and the maximum ITC is just about 1 MW m^{-2} K^{-1} (Figure 7c). Rudimylla et al. found that the contact angles of

Table 2. Thermal bonding materials.

Types	Carriers	Bond types	Mechanism	Typical materials
Metal TBM	Electron dominant	Metal bond, van der Waals force	Increase electron density and electron–phonon coupling	In, Ni, Bi—Zn, Bi—Ag, Sn—Al[97–101]
Organic TBM	Phonon dominant	Covalent bond, hydrogen bond, van der Waals force	Increase overlap of VDOS and bonding strength	$-CH_3$, $-HS$, $-NH_2$, $-OH$, $-COOH$, $-Cl$ SAM[27,102]
Inorganic nonmetal TBM	Phonon dominant	Covalent bond, van der Waals force	Increase electron density, bonding strength and overlap of VDOS	Graphene, AlGaN, SiN, TiC[86,103,104]

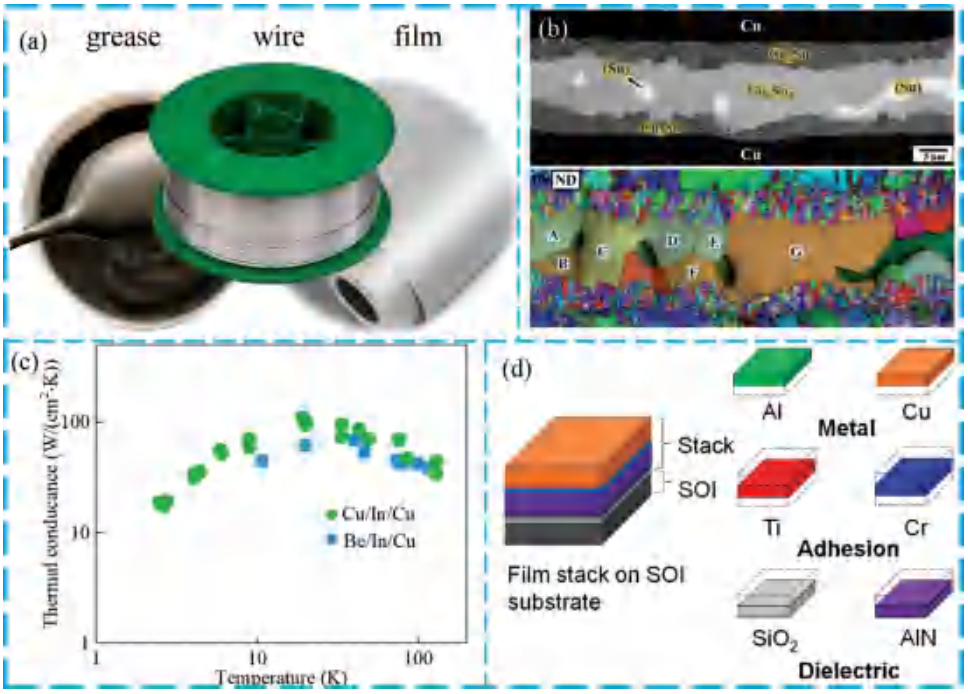

Figure 7. Metal thermal bonding materials. a) Morphology of welding wire, slurry, and film. b) Cross-sectional micrograph of Cu/Sn (10 µm)/Cu sandwich aged at 180 °C for 192 h. Reproduced with permission.[107] Copyright 2014, IEEE. c) Variation of interfacial heat transfer with temperature for Cu/In/Cu and Be/In/Cu. Reproduced with permission.[97] Copyright 2020, AIP Publishing. d) Metal thermal bonding materials at metal–dielectric interfaces. Reproduced with permission.[108] Copyright 2020, American Chemical Society.

Bi–Zn with copper, nickel, invar alloy, and steel increase gradually, and the ITC decreases gradually. Besides, owing to metal TBMs that can transport electrons, they can be used at two carbon nanotubes interface.[106] The experimental results show that the ITC can increase from 0.1 to 1.0 MW m^{-2} K^{-1} by using indium as thermal bonding layer.

An appropriate choice of metal TBMs with relatively strong electron–phonon coupling could significantly enhance interfacial thermal transport across metal–dielectric interfaces.[109,110] The measured ITCs of Ag/diamond and Au/diamond[101] were observed to increase from 45 to 177 MW m^{-2} K^{-1} and from 78 to 208 MW m^{-2} K^{-1} when inserting a 1.5 nm Ni interlayer. It also was found that by using Ti and Cr as inserting materials, the thermal transport across Cu/SiO_2 interface was enhanced, while that of Al/SiO_2 interface changes little[108] (Figure 7d).

4.2. Organic Thermal Bonding Material

Alkane is the main organic TBM. Its chemical composition is A-$(CH_2)_n$-B, and the common functional groups are $-CH_3$, $-HS$, $-OH$, $-COOH$, $-NH_2$, and $-Cl$. The selection of appropriate alkanes can bridge the VDOS of the upper and lower surfaces, and improve the interfacial bonding strength. $-CH_3$ can connect with the upper and lower surfaces by van der Waals force, $-HS$, $-Cl$, and $-NH_2$ can form covalent bonds with metal and alkanes, and $-OH$, and $-COOH$ can form hydrogen bonds with water and alkanes.

The experimental measurements[66] show that when using CH_3-SAM and SH-SAM as bonding materials at the Cu/SiO_2 interface, the ITC can increase three- and four-folds (**Figure 8**a). When using SH-SAM as bonding material at Au/SiO_2, the ITC can increase three times. This is due to the good matching characteristics of such two SAMs with Cu and Au, and the stronger interfacial bonding strength of SH-SAM with Cu and Au. $C_{10}S_2$ is an alkane with $-HS$ groups at both ends, and C_6S, $C_{11}S$, and $C_{14}S$ are alkanes with $-HS$ at one end and $-CH_3$ at one end. $C_{10}S_2$ can covalently bond with gold surfaces, while C_6S, $C_{11}S$, and $C_{14}S$ are covalent bonds on one side and van der Waals force on the other side. By adjusting the ratio of $-CH_3$ group and $-HS$ group, the bonding strength and thermal conduction can be regulated[111] (Figure 8b). OH-SAM and COOH-SAM can easily form hydrogen bonds with water and most organic materials. $HS(CH_2)_6OH$ and $HS(CH_2)_5COOH$ can be used to enhance Au/organic liquids ($C_5H_{11}CH_3$, $C_6H_{13}NH_2$, $C_6H_{13}OH$)[69] (Figure 8c). HS-$(CH_2)_5$-CH_3, $HS(CH_2)_6OH$, and $HS(CH_2)_5COOH$ are the bonding materials for the Au/water interface.[67,112] In the work of Ota et al.,[113] the ITC between Al and the graphite edge can be significantly improved by inserting NH_2-SAM to the interface, which increases the strength of interface bonding (Figure 8d). Cl-SAM is used to modify the liquid metal/copper interface, which improves the thermal conductivity and stability of copper doped liquid metal TIMs, as shown in Figure 8e.[102]

4.3. Inorganic Nonmetal Thermal Bonding Material

Inorganic nonmetal TBMs generally have high melting points, and it is difficult to form strong interactions with other materials at room temperature, usually in the form of van der Waals

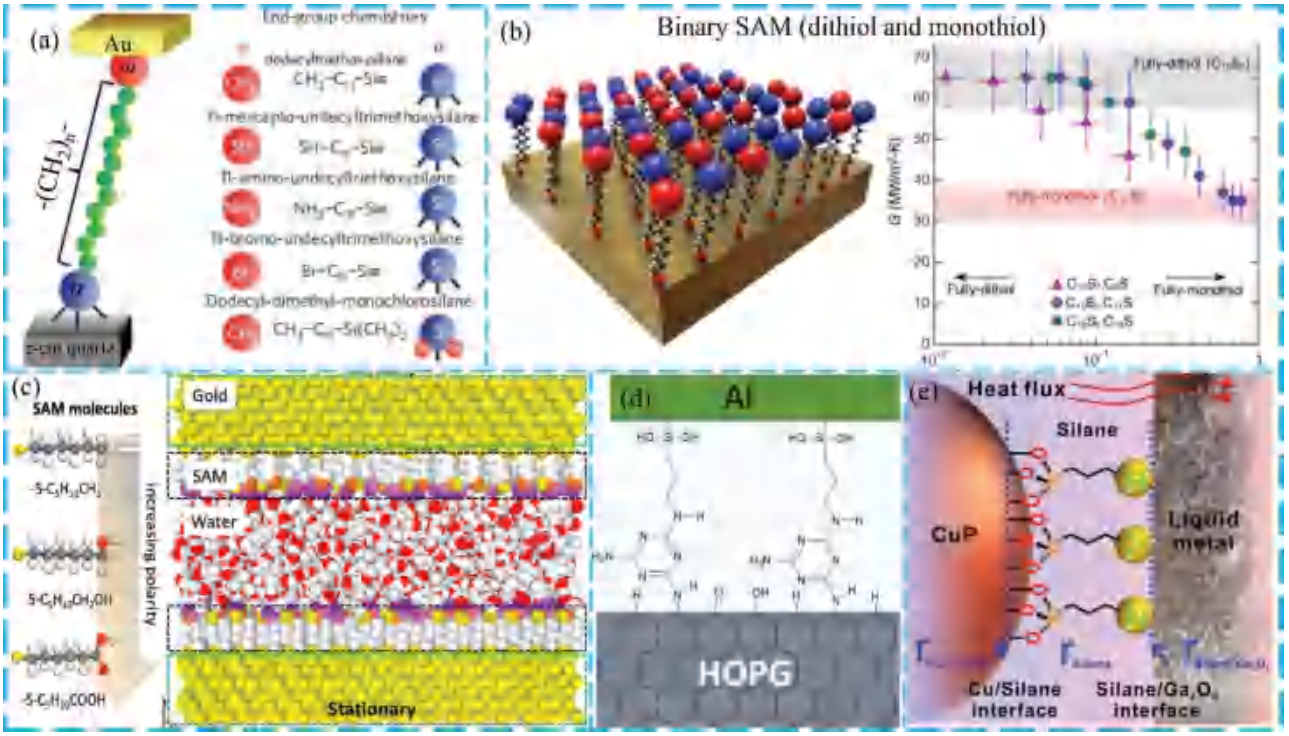

Figure 8. Organic thermal bonding materials. a) Different SAMs at the Au/quartz interface. Reproduced with permission.[66] Copyright 2013, Springer Nature. b) Regulation of interfacial thermal conductance by adjusting the ratio of $-CH_3$ group and $-HS$ group. Reproduced with permission.[111] Copyright 2016, American Chemical Society. c) OH-SAM and COOH-SAM at the Au/H_2O interface.[67] Reproduced with permission.[112] Copyright 2019, American Chemical Society. d) NH_2-SAM at the Al/HOPG interface. Reproduced with permission.[113] Copyright 2019, American Chemical Society. e) Cl-SAM at the liquid metal/Cu interface. Reproduced with permission.[102] Copyright 2021, Wiley-VCH.

force. Han et al.[114] used graphene oxide and amino silane-modified graphene oxide as thermal bonding layers to enhance interfacial heat transfer of Au-Cr/graphene and Au-Cr/silica. It is found that the interfacial thermal resistance of modified graphite oxide/graphene film is four times lower than that of graphite/graphene film, as shown in **Figure 9**a. The interfacial thermal resistance of modified graphite oxide/silica is three times lower than that of graphite/silica.

In the microelectronic manufacturing process, high-temperature treatment and magnetron sputtering preparation are beneficial for covalent bond forming. As the third-generation semiconductor, GaN is now widely used in all kinds of high-power electronic devices.[115,116] Due to the mature growth process and high thermal conductivity, SiC has also become the mainstream substrate material of high-power electronic devices. For all kinds of SiC-based GaN devices, it is very important to improve the thermal conduction of GaN/SiC interface. An interlayer with intermediate phonon spectra between two dielectric materials could reduce the phononic interfacial thermal resistance. Hu et al.[104] analyzed the significant effect of introducing AlN and AlGaN transition layers at the GaN/SiC interface. By introducing AlN transition layer, the interface thermal conduction of GaN/SiC can be increased by 45–55%. $Al_xGa_{(1-x)}N$ can also be used as the bonding layer, and the GaN/SiC ITC increases with the concentration of Al atoms. This is mainly because Al—N covalent bond plays the role of "phonon bridge" near the interface, which effectively makes up for the difference of VDOS between Ga/Si atoms. Diamond is another substrate material for GaN high-power electronic devices for its high thermal conductivity.[117] Zhou et al.[103] reduced the interfacial thermal resistance by introducing bonding layers such as SiN and AlN at the GaN/diamond interface. When SiN is used as a bonding material, the maximum ITC is 150 MW m^{-2} K^{-1}, as shown in Figure 9b. Yote et al. also obtained the largest ITC by inserting a SiN interfacial layer at due to GaN/diamond interface (Figure 9c). The influence of the thickness of β-Ga_2O_3, and the applied power density on the thermal dissipation capabilities of the β-Ga_2O_3-AlN heterostructures is discussed in ref. [118].

5. Applications

5.1. Batteries

The electrochemical performance of lithium-ion battery is limited by the internal heat transfer performance of the battery.[119,120] The experimental results show that interfacial thermal resistance contributes about 88% of the total thermal resistance, which is due to the poor bonding strength and great acoustic mismatch between them.[121] To solve this problem, TBMs have been introduced.[122–124] When the amine end group material is bonded, the interfacial thermal resistance is reduced by four times, while the electrochemical performance has not deteriorated, so that the effective thermal conduction is increased by three times and the maximum peak temperature of the battery is reduced by 60%[125] (**Figure 10**a). Self-assembled

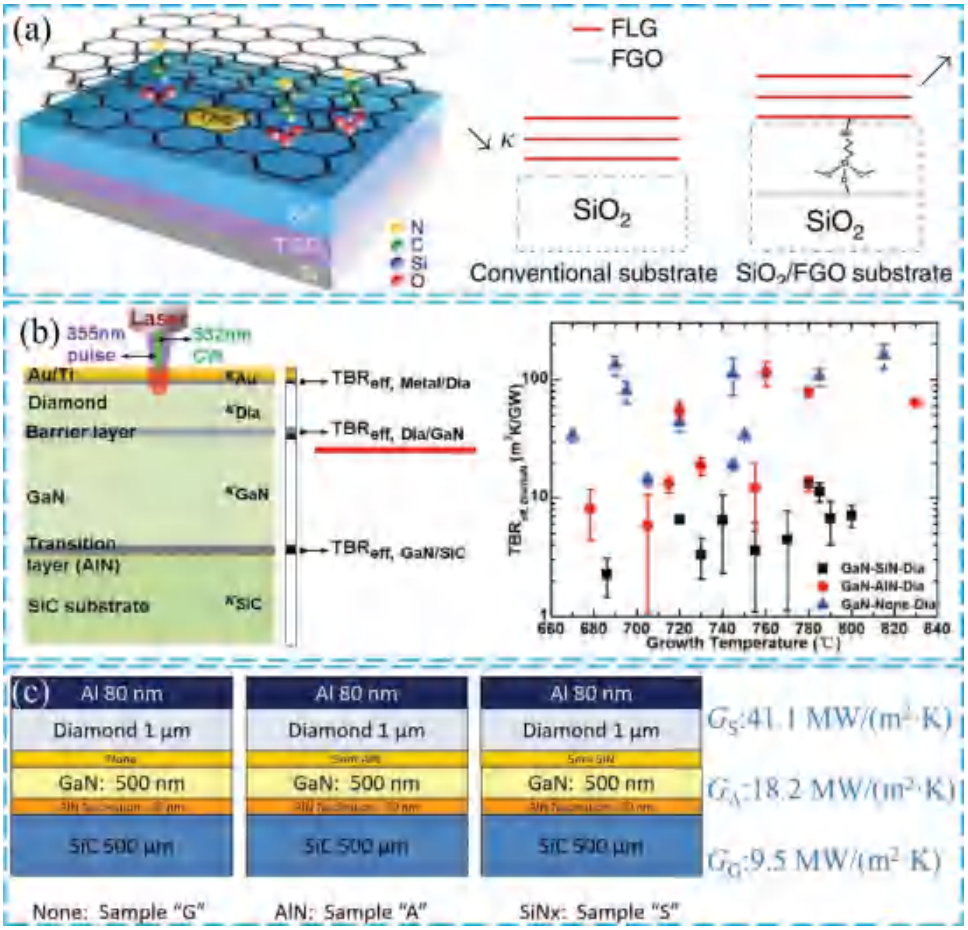

Figure 9. Inorganic nonmetal thermal bonding material. a) Graphene oxide and amino silane-modified graphene oxide for Au-Cr/graphene and Au-Cr/silica. Reproduced under the terms of the CC-BY 4.0 license.[114] Copyright 2016, The Authors, published by Springer Nature. b) TBR of GaN/diamond interfaces with SiN and AlN as bonding layers. Reproduced with permission.[92] Copyright 2018, American Chemical Society. c) ITC of GaN/diamond interfaces with SiN and AlN as bonding layers. Reproduced with permission.[103] Copyright 2017, American Chemical Society.

monolayers polyacrylic acid (PAA), PAM, and PVA are used as bonding materials to form hydrogen bonds with polyethylene oxide (PEO) to enhance the ITC between electrode lithium cobalt oxide (LCO) and solid electrolyte PEO. The simulation results[126] show that compared with LCO-PEO interface, the ITC of LCO/PAA/PEO, LCO/PAM/PEO, and LCO/PVA/PEO increases by 211.69%, 151.99%, and 127.36%, respectively (Figure 10b). Abhijeet et al.[121] calculated the interfacial thermal transport between LCO and amorphous polyethylene when bridged with 3-aminopropyltriethoxysilane (APTES), *n*-butyl trimethoxysilane, and 3-mercaptopropyltrimethoxysilane (MPTMS). The results show that in the case of APTES, molecular bridging at the interface can increase the ITC by 250% (Figure 10c).

5.2. Microelectronic Chips

3D electronic stacked integration is a prospective packaging technology due to its shorter interconnection, higher bandwidth, and lower cost. An important technology to realize 3D stacking is interlayer bonding technology, such as forming electrical, thermal, and mechanical connections through ball grid arrays, microbumps, or bump-free copper bonds, as shown in **Figure 11**a. Copper, gold, and silver are commonly used chip connecting materials. In order to increase the bonding strength, a layer of nickel will be plated on the copper surface in some scenarios. Due to the high melting point of these materials, it is usually necessary to insert a layer of bonding materials with low melting points, such as indium and tin, as shown in Figure 11b.[127] When the temperature is higher than the melting point of the bonding material, the bonding material will form intermetallic compounds with copper, gold, and silver to form a firm mechanical connection, which is conducive to enhancing the interfacial heat transfer.[128–134] However, due to the low thermal conductivity of the intermetallic compounds, it is necessary to control the appropriate thickness. Compared with ball grid array bonding and microbump bonding, Cu—Cu direct bonding without bumps has a smaller connection length, better electrical and thermal properties, and stronger scalability of Cu—Cu bond, and ultrafine spacing can be easily realized by back-end process. The SAM can bond with the copper surface, which can slow down the oxidation and reduce the Cu—Cu bonding temperature, which is called low-temperature

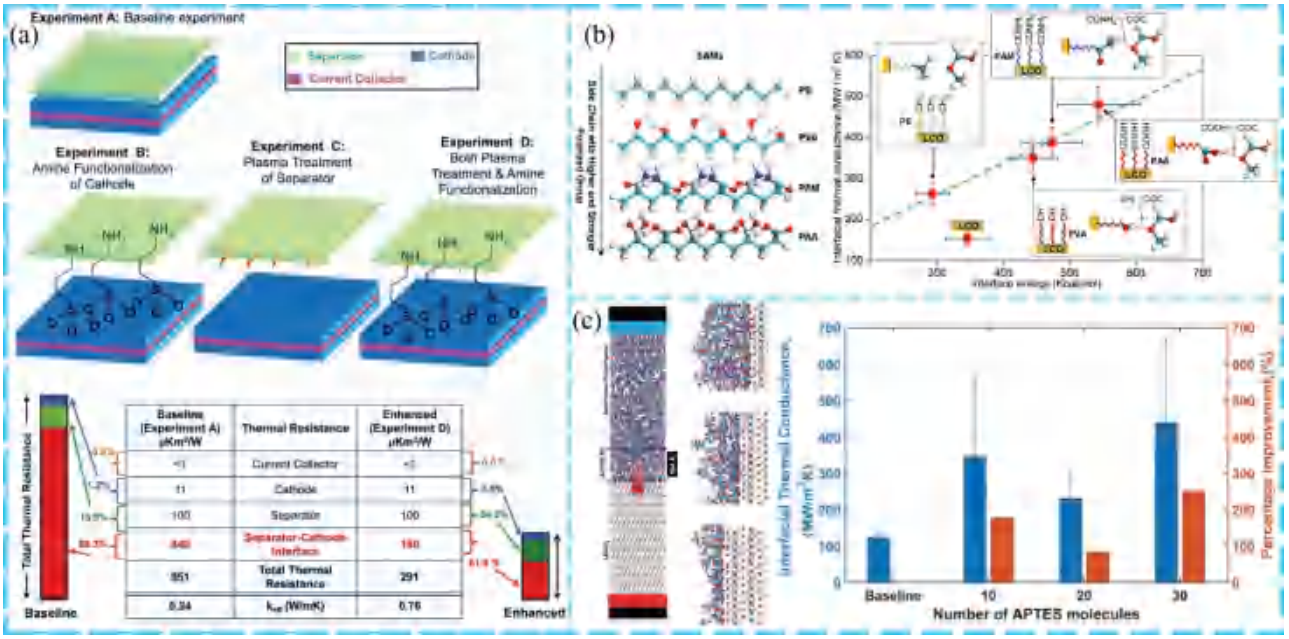

Figure 10. Lithium-ion batteries. a) Amine end group material bonding between separator and cathode. Reproduced with permission.[125] Copyright 2015, Elsevier. b) Self-assembled monolayers PAA, PAM, and PVA bonding with PEO. Reproduced with permission.[126] Copyright 2020, Elsevier BV. c) $LiCoO_2$ and amorphous polyethylene bonding with APTES, *n*-BTMS, and MPTMS. Reproduced with permission.[121] Copyright 2020, Elsevier.

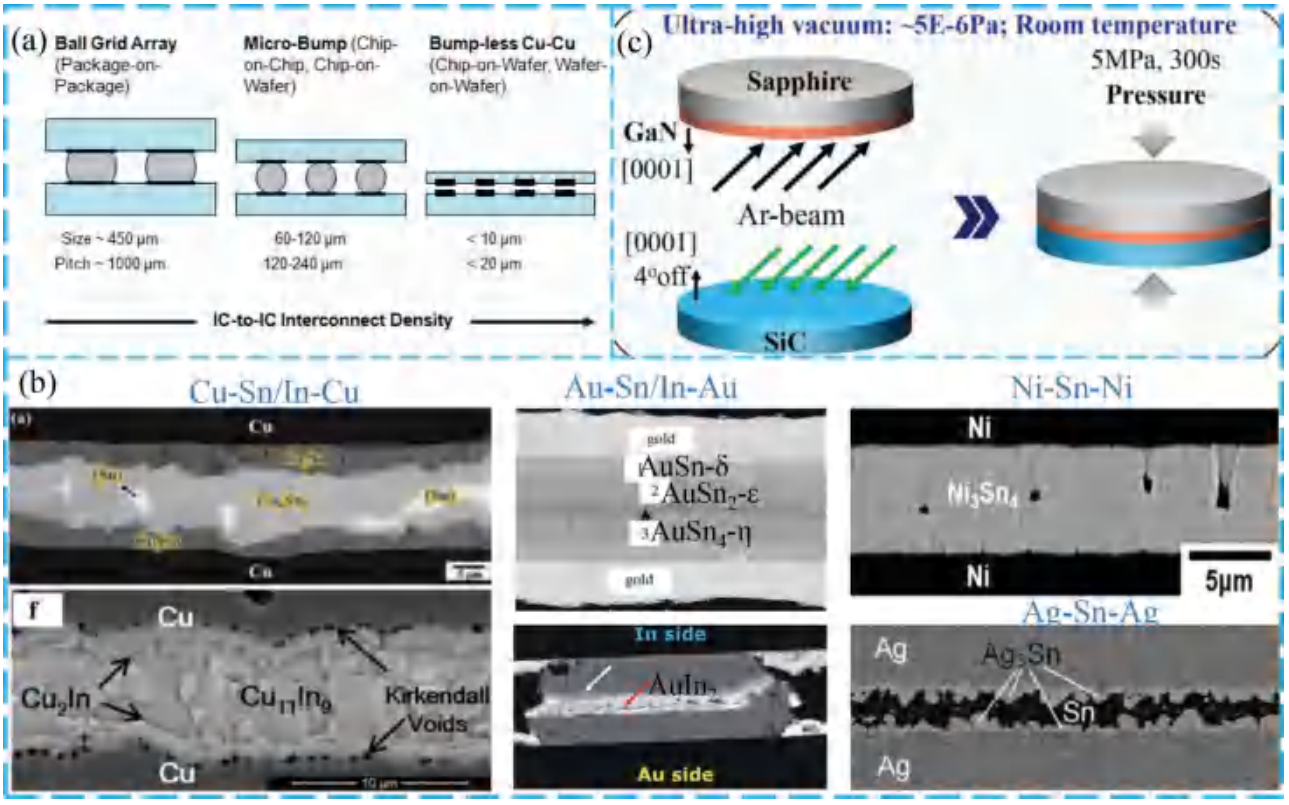

Figure 11. Microelectronic chips. a) 3D stacked packaging. Reproduced with permission.[127] Copyright 2013, The Electrochemical Society. b) Intermetallic compound. Reproduced with permission.[128] Copyright 2010, Elsevier Ltd. Reproduced with permission.[129] Copyright 2014, Springer US. Reproduced with permission.[131] Copyright 2017, Springer US. Reproduced with permission.[132] Copyright 2008, Springer US. Reproduced with permission.[134] Copyright 2014, Springer US. c) Direct room-temperature Ar surface activation. Reproduced with permission.[136] Copyright 2020, American Chemical Society.

bonding.[135] After the copper surface was cleaned, a layer of SAM material was added. During bonding, SAM is desorbed first, and then the hot pressing process can be carried out at low temperature.

The development of GaN-on-diamond substrates holds much promise for the creation of high-power density electronics. Increasing the interfacial thermal transport between GaN and SiC will aid in the heat dissipation of GaN-on-SiC devices. A high ITC of GaN/SiC was obtained by direct room-temperature Ar surface activation,[136] measured 230 MW m^{-2} K^{-1} (Figure 11c). Yates et al.[92] explored the role of different interfaces in contributing to the interfacial thermal resistance of GaN/diamond layers, specifically using 5 nm layers of AlN, SiN, or no interlayer at all. It found that SiN interfacial layer provided the lowest interfacial thermal resistance (<10 m^2 K GW^{-1}) because of the formation of a Si–C–N layer at the interface.

5.3. Thermal Management Materials

With the continuous improvement of electronic integration, there is an urgent need for thermal management materials to meet the needs of high heat flux.[13,137–141] Zhang[142] and Shanker[138] studied the relationship between the thermal conductivity of amorphous polymers and intermolecular bonding force. The simulation results showed that the greater the interfacial bonding force was, the greater the thermal conductivity of polyethylene (**Figure 12**a). Using polymer mixing to increase the interaction between polymers can improve thermal conductivity. Kim et al.[143] found that PAA was doped with 30% poly(*N*-acryloyl piperidine) (PAP), PAA and PAP were connected by hydrogen bonds, and the planar thermal conductivity could reach 1.5 W m^{-1} K^{-1}) (Figure 12b). The interfacial force between graphene and polymer is very poor, and the interfacial bonding strength can be improved by bonding materials. Song et al.[144] first grew a layer of polydopamine (PDA) on the surface of polypropylene (PP), and then plated a layer of graphene on the surface of PDA. PDA is connected with PP by hydrogen bond and graphene by covalent bond, which significantly improves the interfacial bonding strength. The in-plane thermal conductivity of the material is 10.93 W m^{-1} K^{-1}, which is 55 times that of pure PP and four times that of PP/graphene (Figure 12c).

In addition, adding fillers with high thermal conductivity to polymers is also a way to improve thermal conductivity. Boron nitride is an insulating material with high thermal conductivity, which is used as a thermally conductive filler. However, there is no bond between boron nitride and organic materials, and the interfacial thermal resistance is large.[146,147] By modifying BN with hydroxyl or carboxyl groups, the bonding strength

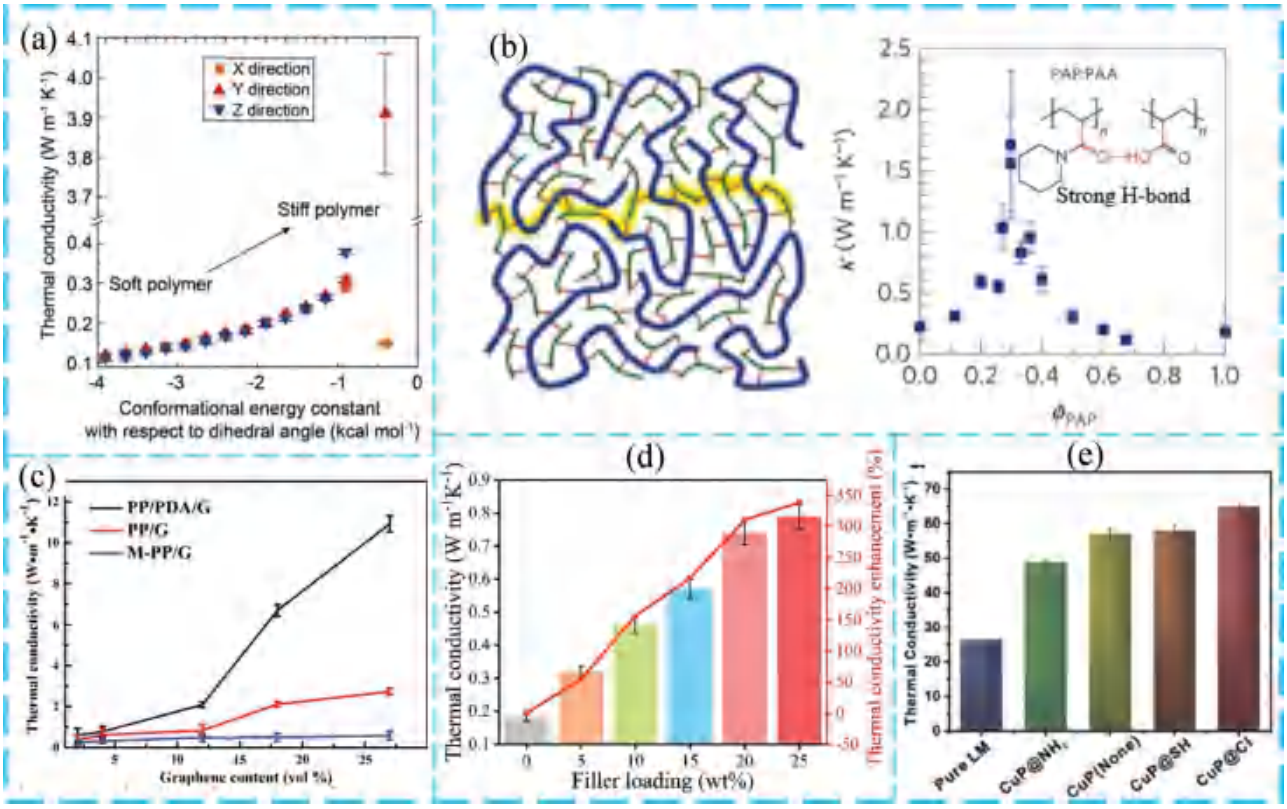

Figure 12. Thermal management materials. a) The relationship between the thermal conductivity of amorphous polymers and intermolecular bonding force. Reproduced with permission.[142] Copyright 2016, American Chemical Society. b) Polymer mixing to increase the interaction between polymers. Reproduced with permission.[143] Copyright 2015, Springer Nature. c) Polydopamine is connected with polypropylene and graphene. Reproduced with permission.[144] Copyright 2020, Elsevier Ltd. d) BN is modified with hydroxyl or carboxyl groups. Reproduced with permission.[145] Copyright 2020, Elsevier Ltd. e) Organic SAM bonds copper and liquid metal. Reproduced with permission.[102] Copyright 2021, Wiley-VCH. The abbreviations of PAA, PAP, PDA, and PP are polyacrylic acid, poly(*N*-acryloyl piperidine), polydopamine, and polypropylene.

with organic materials and the thermal conductivity of materials can be increased (Figure 12d).[145] Liquid metal is a kind of TIM.[102] In order to further improve the thermal conductivity of liquid metal gallium indium alloy, doping can be realized. However, due to the formation of intermetallic compounds between copper and gallium, the expected thermal conductivity is reduced. Therefore, plating an organic monolayer on the surface of copper can not only increase the interfacial bonding force and improve the thermal conductivity, but also avoid corrosion between copper and gallium (Figure 12e).

6. Summary and Outlook

Interfacial heat transfer barrier is currently becoming ubiquitous in energy conversion and transport applications with characteristic dimensions approaching nanoscale. Sandwiching an intermediate material between two materials can enhance electron and phonon transmission, and it has in fact gathered substantial attention. This article summarizes and comprehensively interprets previous typical researches regarding such a strategy. Additionally, we name this method as thermal bonding and first systematically classify TBMs into three categories: metal TBM, organic TBM, and inorganic nonmetal TBM.

The above discussions illustrate exciting progress in pursuing the extremes of large ITC. As a novel and promising interface science and engineering field, we believe that thermal bonding strategy will provide scientists and engineers more inspiration to solve the interfacial heat transfer challenges faced by a large number of micro/nano heat transfer applications. In the near future, some major directions that may guide future research are outlined as follows.

6.1. Interfacial Heat Transport Physics between Different Heat Carriers

To be exact, although phonon successfully describes energy transfer in crystals, its validity cannot be extended in water and many amorphous solids, like polymers, gels, a-Si, and glass, due to lack of periodic long-range order. Wave-like tunneling conduction mechanism, named diffusons[148,149] or coherences,[150] has been proved to be dominant in amorphous solids and non-negligible in low-thermal conductivity complex crystals. The tunneling conduction is from coherences between pairs of vibrational modes, assuming great importance when the mode linewidths are comparable to or larger than the interbranch spacings, which is beyond the well-established phonon Boltzmann transport equation. The harmonic Allen–Feldman theory,[151] the quasi-harmonic Green–Kubo model,[152] and the Wigner transport equation[149] have been developed to consider the tunneling conduction and provided deep understanding of the heat conduction in terms of the temperature dependence,[153–155] anharmonicity,[156] and disorder.[152] The wave-like tunneling conduction mechanism might offer new insight for interfacial heat transfer because defects, amorphous buffer/transition layer, and other complex structures are common in the interfacial region, as well as the tunneling conduction possesses increasing significance with disordering. Various heat carriers, including phonons, diffusons, electrons, and interface phonon polaritons might coexist in practical interfaces so their interactions are necessary to be considered. How to include the new mechanisms and complex interactions is challenging, meaningful, and of great interest.

6.2. Describing Intricate and Ticklish Practical Interfacial Structures

The interfacial heat transfer model is crucial for selecting TBMs and designing interfacial structures. However, AMM, DMM, and other models only consider A/B interface within the author's knowledge. There is no research on the A/T/B interface heat transfer model, where T is a TBM. Therefore, the basic three-layer interfacial heat transfer needs to be investigated. In addition, the interaction models for different types of heat carriers are urgently needed to develop.

6.3. Increasing Electron Transmission for the Metal–Nonmetal Interface

As mentioned in Section 2, electron heat transfer plays an important role at the metal–nonmetal interface, so it is necessary to strengthen the electron transport at the metal/nonmetal interface. However, for metal/nonmetal interface bonding, alkane materials are usually used as bonding materials to enhance phonon transmission at the interface. It ignores the effect of electron heat transfer. Therefore, it is very important to find materials that enhance both electron and phonon transmission to further enhance metal–nonmetal interfacial heat transfer.

6.4. Screening More Thermal Bonding Materials

TBMs are the key for thermal bonding strategy, while currently, the available TBMs are few. The experimental method is used to compare the thermal conductance of existing TBMs, while it consumes much time and money. The slow experimental test cannot meet the urgent aspiration for TBMs. With the maturity of atomistic simulation methods, the high-throughput screening of materials with extremely high thermal conductivity currently becomes possible.[157,158] Although state-of-the-art density functional theory (DFT) methods can model materials with quantum-mechanical accuracy, it would be infeasible to tackle interfacial problems due to unaffordable computational costs. With the recent emergence of machine learning interatomic potentials that enable simulations with an accuracy closer to DFT, but with linear scaling behavior, machine learning-driven materials modeling is promising to become a powerful tool in describing interfacial thermal transport properties and ultimately accelerating high-throughput screening of TBMs.[159–161]

6.5. Codesign of Mechanical Bonding-Electrical Bonding-Thermal Bonding

With enhancing the interfacial heat transfer capability, thermal bonding will also change the mechanical and electrical properties of the interface. Large interfacial adhesion energy will

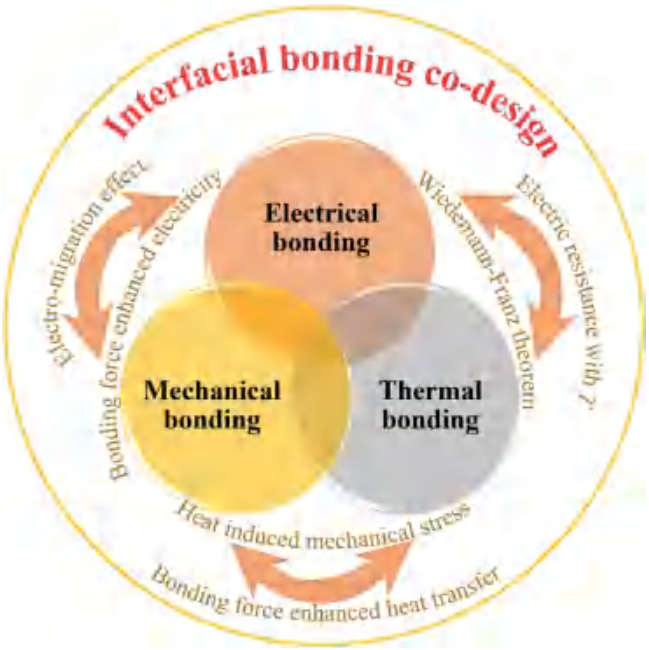

Figure 13. Codesign of mechanical bonding-electrical bonding-thermal bonding.

enlarge the ITC, but it will also increase the mechanical adhesion of the interface, and increase the interfacial electric conductance. Therefore, mechanical bonding, electrical bonding, and thermal bonding are coupled at interface (**Figure 13**). For the bonding between chip and substrate, large interface thermal conduction, electrical conduction, and mechanical adhesion are simultaneously pursued. For thermal packaging polymers, large interfacial thermal conduction, small electrical conduction, and certain hardness are required. For nanodoped thermal conductive silicone grease, it pursues large interfacial thermal conduction, small interfacial electrical conductivity, and viscosity. Therefore, the codesign of mechanical bonding-electrical bonding-thermal bonding needs to be seriously considered for different applications.

Acknowledgements

This work was supported by National Natural Science Foundation of China (Grant Nos. 51825601 and U20A20301) and China Postdoctoral Science Foundation (Grant No. 2021M701852).

Conflict of Interest

The authors declare no conflict of interest.

Keywords

interaction forces, interfacial thermal transport, phonon vibration density of states, single alkane molecule, thermal bonding

Received: January 12, 2022
Revised: April 18, 2022
Published online: August 29, 2022

[1] A. Giri, P. E. Hopkins, *Adv. Funct. Mater.* **2019**, *30*, 1903857.
[2] D. G. Cahill, P. V. Braun, G. Chen, D. R. Clarke, S. Fan, K. E. Goodson, P. Keblinski, W. P. King, G. D. Mahan, A. Majumdar, H. J. Maris, S. R. Phillpot, E. Pop, L. Shi, *Appl. Phys. Rev.* **2014**, *1*, 011305.
[3] G. Chen, *Nat. Rev. Phys.* **2021**, *3*, 555.
[4] L. Cui, S. Hur, Z. A. Akbar, J. C. Klockner, W. Jeong, F. Pauly, S. Y. Jang, P. Reddy, E. Meyhofer, *Nature* **2019**, *572*, 628.
[5] M. G. Rosul, D. Lee, D. H. Olson, N. Liu, X. Wang, P. E. Hopkins, K. Lee, M. Zebarjadi, *Sci. Adv.* **2019**, *5*, eaax7827.
[6] K. Ren, X. J. Liu, S. Chen, Y. Cheng, W. C. Tang, G. Zhang, *Adv. Funct. Mater.* **2020**, *30*, 2004003.
[7] A. Sarua, H. Ji, K. P. Hilton, D. J. Wallis, M. J. Uren, T. Martin, M. Kuball, *IEEE Trans. Electron Dev.* **2007**, *54*, 3152.
[8] O. O. S. Kang, M. Li, H. Wu, H. Nguyen, T. Aoki, Y. J. Hu, *Nat. Electron.* **2021**, *4*, 416.
[9] Z. Cheng, J. Shi, C. Yuan, S. Kim, S. Graham, *Semicond. Semimetals* **2021**, *107*, 77.
[10] S. D. Lubner, S. Kaur, Y. B. Fu, V. Battaglia, R. S. Prasher, *J. Appl. Phys.* **2020**, *127*, 105104.
[11] A. G. Ricciardulli, S. Yang, J. H. Smet, M. Saliba, *Nat. Mater.* **2021**, *20*, 1325.
[12] S. Lou, F. Zhang, C. Fu, M. Chen, Y. Ma, G. Yin, J. Wang, *Adv. Mater.* **2021**, *33*, 2000721.
[13] X. Qian, J. Zhou, G. Chen, *Nat. Mater.* **2021**, *20*, 1188.
[14] K. M. Razeeb, E. Dalton, G. L. W. Cross, A. J. Robinson, *Int. Mater. Rev.* **2017**, *63*, 1.
[15] C. Liu, W. Yu, C. Chen, H. Xie, B. Cao, *Int. J. Heat Mass Transfer* **2020**, *163*, 120393.
[16] J. L. West, N. J. Halas, *Annu. Rev. Biomed. Eng.* **2003**, *5*, 285.
[17] S. K. Das, S. U. Choi, W. Yu, T. Pradeep, *Nanofluids: Science and Technology*, John Wiley & Sons, New York **2007**.
[18] Z. T. Zhang, R. Y. Dong, D. S. Qiao, B. Y. Cao, *Nanotechnology* **2020**, *31*, 465403.
[19] B. Y. Cao, J. H. Zou, G. J. Hu, G. X. Cao, *Appl. Phys. Lett.* **2018**, *112*, 041603.
[20] Devender, K. Lofgreen, S. Devasenathipathy, J. Swan, R. Mahajan, T. Borca-Tasciuc, G. Ramanath, *J. Vac. Sci. Technol., A* **2015**, *33*, 060611.
[21] S. Kanetsuki, S. Miyake, K. Kuwahara, T. Namazu, *Jpn. J. Appl. Phys.* **2016**, *55*, 06GP17.
[22] M. A. Raza, A. V. K. Westwood, A. P. Brown, C. Stirling, *J. Mater. Sci.: Mater. Electron.* **2012**, *23*, 1855.
[23] S. Narumanchi, presented at *11th Intersociety Conf. on Thermal and Thermomechanical Phenomena in Electronic Systems*, Orlando, FL, USA, May **2008**.
[24] R. Zhang, J. Cai, Q. Wang, J. W. Li, Y. Hu, H. D. Du, L. L. Li, *J. Electron. Packag.* **2014**, *136*, 011012.
[25] H. Liu, D. Grasseschi, A. Dodda, K. Fujisawa, D. Olson, E. Kahn, F. Zhang, T. Zhang, Y. Lei, R. B. N. Branco, *Sci. Adv.* **2020**, *6*, eabc9308.
[26] X. S. Liu, R. W. Davis, L. C. Hughes, M. H. Rasmussen, R. Bhat, C. E. Zah, J. Stradling, *J. Appl. Phys.* **2006**, *100*, 013104.
[27] S. Park, J. Jang, H. Kim, D. I. Park, K. Kim, H. J. Yoon, *J. Mater. Chem. A* **2020**, *8*, 19746.
[28] T. C. Wei, A. R. Daud, *J. Electron. Packag.* **2003**, *125*, 617.
[29] L. Zhang, G. Wang, Y. Zhang, Z. Cao, Y. Wang, T. Cao, C. Wang, B. Cheng, W. Zhang, X. Wan, J. Lin, S. J. Liang, F. Miao, *ACS Nano* **2020**, *14*, 10265.
[30] J. S. Ha, S. I. Hong, *Mater. Des.* **2013**, *51*, 293.
[31] P. E. Hopkins, *Int. Scholarly Res. Not.* **2013**, *2013*, 682586.
[32] E. T. Swartz, R. O. Pohl, *Rev. Mod. Phys.* **1989**, *61*, 605.
[33] S. Pettersson, G. D. Mahan, *Phys. Rev. B* **1990**, *42*, 7386.
[34] M. M. Yovanovich, *IEEE Trans. Compon. Packag. Technol.* **2005**, *28*, 182.

[35] H. Subramanyan, K. Kim, T. Y. Lu, J. Zhou, J. Liu, *AIP Adv.* **2019**, *9*, 115116.
[36] A. N. S. Robert, J. Stevens, P. M. Norris, *J. Heat Transfer* **2005**, *127*, 315.
[37] P. E. Hopkins, J. C. Duda, P. M. Norris, *J. Heat Transfer* **2011**, *133*, 062401.
[38] W. Zhang, T. Fisher, N. Mingo, *Numer. Heat Transfer, Part B* **2007**, *51*, 333.
[39] W. Zhang, T. Fisher, N. Mingo, *J. Heat Transfer* **2007**, *129*, 489.
[40] J.-S. Wang, J. Wang, J. Lü, *Eur. Phys. J. B* **2008**, *62*, 381.
[41] S. Sadasivam, Y. Che, Z. Huang, L. Chen, S. Kumar, T. S. Fisher, *Annu. Rev. Heat Transfer* **2014**, *17*, 89.
[42] J. Dai, Z. Tian, *Phys. Rev. B* **2020**, *101*, 041301.
[43] Y. Guo, Z. Zhang, M. Bescond, S. Xiong, M. Nomura, S. Volz, *Phys. Rev. B* **2021**, *103*, 174306.
[44] Y. Chalopin, A. Rajabpour, H. Han, Y. Ni, S. Volz, *Annu. Rev. Heat Transfer* **2014**, *17*, 147.
[45] E. Landry, A. McGaughey, *Phys. Rev. B* **2009**, *80*, 165304.
[46] K. Gordiz, A. Henry, *Sci. Rep.* **2016**, *6*, 23139.
[47] K. Gordiz, A. Henry, *New J. Phys.* **2015**, *17*, 103002.
[48] K. Sääskilahti, J. Oksanen, J. Tulkki, S. Volz, *Phys. Rev. B* **2014**, *90*, 134312.
[49] Y. Zhou, M. Hu, *Phys. Rev. B* **2017**, *95*, 115313.
[50] Y. Yao, J. Fry, M. E. Fine, L. M. Keer, *Acta Mater.* **2013**, *61*, 1525.
[51] R. B. Wilson, D. G. Cahill, *Phys. Rev. Lett.* **2012**, *108*, 255901.
[52] D. W. Oh, S. Kim, J. A. Rogers, D. G. Cahill, S. Sinha, *Adv. Mater.* **2011**, *23*, 5028.
[53] J. Ordonez-Miranda, J. J. Alvarado-Gil, R. Yang, *J. Appl. Phys.* **2011**, *109*, 094310.
[54] A. Giri, J. T. Gaskins, B. F. Donovan, C. Szwejkowski, R. J. Warzoha, M. A. Rodriguez, J. Ihlefeld, P. E. Hopkins, *J. Appl. Phys.* **2015**, *117*, 105105.
[55] A. Majumdar, P. Reddy, *Appl. Phys. Lett.* **2004**, *84*, 4768.
[56] Y. S. Ju, *J. Heat Transfer* **2005**, *127*, 1400.
[57] Z. Lu, Y. Wang, X. Ruan, *Phys. Rev. B* **2016**, *93*, 225109.
[58] M. J. Li, Y. Y. Wang, J. Zhou, J. Ren, B. W. Li, *Eur. Phys. J. B* **2015**, *88*, 149.
[59] S. Sadasivam, N. Ye, J. P. Feser, J. Charles, K. Miao, T. Kubis, T. S. Fisher, *Phys. Rev. B* **2017**, *95*, 085310.
[60] N. Ye, J. P. Feser, S. Sadasivam, T. S. Fisher, T. Wang, C. Ni, A. Janotti, *Phys. Rev. B* **2017**, *95*, 085430.
[61] Y. R. Koh, J. Shi, B. Wang, R. Hu, H. Ahmad, S. Kerdsongpanya, E. Milosevic, W. A. Doolittle, D. Gall, Z. Tian, *Phys. Rev. B* **2020**, *102*, 205304.
[62] Z. Cheng, Y. R. Koh, H. Ahmad, R. Hu, J. Shi, M. E. Liao, Y. Wang, T. Bai, R. Li, E. Lee, *Commun. Phys.* **2020**, *3*, 115.
[63] H.-K. Lyeo, D. G. Cahill, *Phys. Rev. B* **2006**, *73*, 144301.
[64] Y. Ge, Y. Zhou, T. S. Fisher, *J. Appl. Phys.* **2021**, *130*, 235108.
[65] M. D. Losego, M. E. Grady, N. R. Sottos, D. G. Cahill, P. V. Braun, *Nat. Mater.* **2012**, *11*, 502.
[66] P. J. O'Brien, S. Shenogin, J. Liu, P. K. Chow, D. Laurencin, P. H. Mutin, M. Yamaguchi, P. Keblinski, G. Ramanath, *Nat. Mater.* **2013**, *12*, 118.
[67] D. Huang, R. Ma, T. Zhang, T. Luo, *ACS Appl. Mater. Interfaces* **2018**, *10*, 28159.
[68] R. J. Stoner, H. J. Maris, *Phys. Rev. B* **1993**, *48*, 16373.
[69] T. Zhang, A. R. Gans-Forrest, E. Lee, X. Zhang, C. Qu, Y. Pang, F. Sun, T. Luo, *ACS Appl. Mater. Interfaces* **2016**, *8*, 33326.
[70] B. C. Gundrum, D. G. Cahill, R. S. Averback, *Phys. Rev. B* **2005**, *72*, 245426.
[71] J. Zhong, Q. Xi, Z. Wang, T. Nakayama, X. Li, J. Liu, J. Zhou, *J. Appl. Phys.* **2021**, *129*, 195102.
[72] M. D. Losego, L. Moh, K. A. Arpin, D. G. Cahill, P. V. Braun, *Appl. Phys. Lett.* **2010**, *97*, 011908.
[73] O. M. Wilson, X. Y. Hu, D. G. Cahill, P. V. Braun, *Phys. Rev. B* **2002**, *66*, 224301.
[74] S. T. Huxtable, D. G. Cahill, S. Shenogin, L. Xue, R. Ozisik, P. Barone, M. Usrey, M. S. Strano, G. Siddons, M. Shim, P. Keblinski, *Nat. Mater.* **2003**, *2*, 731.
[75] F. Sun, T. Zhang, M. M. Jobbins, Z. Guo, X. Zhang, Z. Zheng, D. Tang, S. Ptasinska, T. Luo, *Adv. Mater.* **2014**, *26*, 6093.
[76] Z. Ge, D. G. Cahill, P. V. Braun, *Phys. Rev. Lett.* **2006**, *96*, 186101.
[77] A. J. Schmidt, J. D. Alper, M. Chiesa, G. Chen, S. K. Das, K. Hamad-Schifferli, *J. Phys. Chem. C* **2008**, *112*, 13320.
[78] M. Seong, I. Hwang, S. Park, H. Jang, G. Choi, J. Kim, S. K. Kim, G. H. Kim, J. Yeo, H. E. Jeong, *Adv. Funct. Mater.* **2021**, *31*, 2107023.
[79] R. Prasher, *Appl. Phys. Lett.* **2009**, *94*, 041905.
[80] A. G. Slepnev, *Phys. Solid State* **2017**, *59*, 1468.
[81] K. Zheng, F. Sun, X. Tian, J. Zhu, Y. Ma, D. Tang, F. Wang, *ACS Appl. Mater. Interfaces* **2015**, *7*, 23644.
[82] L. Zhang, Z. T. Bai, L. Liu, *Adv. Mater. Interfaces* **2016**, *3*, 1600211.
[83] W. M. Waller, J. W. Pomeroy, D. Field, E. J. Smith, P. W. May, M. Kuball, *Semicond. Sci. Technol.* **2020**, *35*, 095021.
[84] W. Park, T. Kodama, J. Park, J. Cho, A. Sood, M. T. Barako, M. Asheghi, K. E. Goodson, *ACS Appl. Mater. Interfaces* **2017**, *9*, 30100.
[85] J. Shi, C. Yuan, H. L. Huang, J. Johnson, C. Chae, S. Wang, R. Hanus, S. Kim, Z. Cheng, J. Hwang, S. Graham, *ACS Appl. Mater. Interfaces* **2021**, *13*, 29083.
[86] Z. Cheng, L. Yates, J. Shi, M. J. Tadjer, K. D. Hobart, S. Graham, *APL Mater.* **2019**, *7*, 031118.
[87] Y. Song, D. Shoemaker, J. H. Leach, C. McGray, H.-L. Huang, A. Bhattacharyya, Y. Zhang, C. U. Gonzalez-Valle, T. Hess, S. Zhukovsky, *ACS Appl. Mater. Interfaces* **2021**, *13*, 40817.
[88] Z. Cheng, F. Mu, T. You, W. Xu, J. Shi, M. E. Liao, Y. Wang, K. Huynh, T. Suga, M. S. Goorsky, *ACS Appl. Mater. Interfaces* **2020**, *12*, 44943.
[89] Z. Cheng, F. Mu, X. Ji, T. You, W. Xu, T. Suga, X. Ou, D. G. Cahill, S. Graham, *ACS Appl. Mater. Interfaces* **2021**, *13*, 31843.
[90] K. Zheng, F. Sun, X. Tian, J. Zhu, Y. Ma, D. Tang, F. Wang, *ACS Appl. Mater. Interfaces* **2015**, *7*, 23644.
[91] H. Harikrishna, W. A. Ducker, S. T. Huxtable, *Appl. Phys. Lett.* **2013**, *102*, 251606.
[92] L. Yates, J. Anderson, X. Gu, C. Lee, T. Bai, M. Mecklenburg, T. Aoki, M. S. Goorsky, M. Kuball, E. L. Piner, S. Graham, *ACS Appl. Mater. Interfaces* **2018**, *10*, 24302.
[93] H. Zheng, K. Jagannadham, *Metall. Mater. Trans. A* **2014**, *45*, 2480.
[94] B. Xu, S. Hu, S.-W. Hung, C. Shao, H. Chandra, F.-R. Chen, T. Kodama, J. Shiomi, *Sci. Adv.* **2021**, *7*, eabf8197.
[95] R. Y. Wang, R. A. Segalman, A. Majumdar, *Appl. Phys. Lett.* **2006**, *89*, 173113.
[96] J. P. Freedman, J. H. Leach, E. A. Preble, Z. Sitar, R. F. Davis, J. A. Malen, *Sci. Rep.* **2013**, *3*, 2963.
[97] R. Radebaugh, *Rev. Sci. Instrum.* **1977**, *48*, 93.
[98] R. Septimio, C. Cruz, M. Xavier, T. Lima, A. Garcia, J. E. Spinelli, N. Cheung, *Int. J. Therm. Sci.* **2021**, *160*, 106685.
[99] B. L. Silva, F. Bertelli, M. V. Canté, J. E. Spinelli, N. Cheung, A. Garcia, *J. Mater. Sci.: Mater. Electron.* **2015**, *27*, 1994.
[100] R. Oliveira, C. Cruz, A. Barros, F. Bertelli, J. E. Spinelli, A. Garcia, N. Cheung, *J. Therm. Anal. Calorim.* **2022**, *147*, 4945.
[101] M. Blank, G. Schneider, J. Ordonez-Miranda, L. Weber, *J. Appl. Phys.* **2019**, *126*, 165302.
[102] H. Wang, W. Xing, S. Chen, C. Song, M. D. Dickey, T. Deng, *Adv. Mater.* **2021**, *33*, 2103104.
[103] Y. Zhou, J. Anaya, J. Pomeroy, H. Sun, X. Gu, A. Xie, E. Beam, M. Becker, T. A. Grotjohn, C. Lee, M. Kuball, *ACS Appl. Mater. Interfaces* **2017**, *9*, 34416.
[104] M. Hu, X. Zhang, D. Poulikakos, C. P. Grigoropoulos, *Int. J. Heat Mass Transfer* **2011**, *54*, 5183.

[105] V. R. Manikam, K. Y. Cheong, *IEEE T. Comp. Pack. Man.* **2011**, *1*, 457.
[106] T. Tong, Y. Zhao, L. Delzeit, A. Kashani, M. Meyyappan, A. Majumdar, *IEEE Trans. Compon., Packag., Manuf. Technol.* **2007**, *30*, 92.
[107] T. Yang, presented at *2014 IEEE 64th Electronic Components and Technology Conf. (ECTC)*, Orlando, FL, USA, May **2014**.
[108] T. Zhan, S. Ma, Z. Jin, H. Takezawa, K. Mesaki, M. Tomita, Y.-J. Wu, Y. Xu, T. Matsukawa, T. Matsuki, *ACS Appl. Mater. Interfaces* **2020**, *12*, 34441.
[109] S. M. Oommen, S. Pisana, *J. Phys.: Condens. Matter* **2020**, *33*, 085702.
[110] Y. Wang, Z. X. Lu, A. K. Roy, X. L. Ruan, *J. Appl. Phys.* **2016**, *119*, 065103.
[111] S. Majumdar, J. A. Malen, A. J. McGaughey, *Nano Lett.* **2017**, *17*, 220.
[112] D. Huang, T. Zhang, G. Xiong, L. Xu, Z. Qu, E. Lee, T. Luo, *ACS Appl. Mater. Interfaces* **2019**, *11*, 32481.
[113] A. Ota, M. Ohnishi, H. Oshima, T. Shiga, T. Kodama, J. Shiomi, *ACS Appl. Mater. Interfaces* **2019**, *11*, 37295.
[114] H. Han, Y. Zhang, N. Wang, M. K. Samani, Y. Ni, Z. Y. Mijbil, M. Edwards, S. Xiong, K. Saaskilahti, M. Murugesan, Y. Fu, L. Ye, H. Sadeghi, S. Bailey, Y. A. Kosevich, C. J. Lambert, J. Liu, S. Volz, *Nat. Commun.* **2016**, *7*, 11281.
[115] S. B. Reese, T. Remo, J. Green, A. Zakutayev, *Joule* **2019**, *3*, 903.
[116] Y. C. Hua, H. L. Li, B. Y. Cao, *IEEE Trans. Electron Devices* **2019**, *66*, 3296.
[117] Z. Cheng, F. Mu, L. Yates, T. Suga, S. Graham, *ACS Appl. Mater. Interfaces* **2020**, *12*, 8376.
[118] G. Wang, Y. Zhou, *IEEE Trans. Compon., Packag., Manuf. Technol.* **2022**, https://doi.org/10.1109/TCPMT.2022.3157672.
[119] W. Wu, S. Wang, W. Wu, K. Chen, S. Hong, Y. Lai, *Energy Convers. Manage.* **2019**, *182*, 262.
[120] D. Atkins, E. Ayerbe, A. Benayad, F. G. Capone, E. Capria, I. E. Castelli, I. Cekic-Laskovic, R. Ciria, L. Dudy, K. Edström, M. R. Johnson, H. Li, J. M. G. Lastra, M. L. De Souza, V. Meunier, M. Morcrette, H. Reichert, P. Simon, J.-P. Rueff, J. Sottmann, W. Wenzel, A. Grimaud, *Adv. Energy Mater.* **2021**, 2102687, https://doi.org/10.1002/aenm.202102687.
[121] A. Dhakane, V. Varshney, J. Liu, H. Heinz, A. Jain, *Surf. Interfaces* **2020**, *21*, 100674.
[122] R. Yi, Y. Mao, Y. Shen, L. Chen, *J. Am. Chem. Soc.* **2021**, *143*, 12897.
[123] X. Wei, R. Ma, T. Luo, *J. Phys. Chem. C* **2020**, *124*, 4483.
[124] X. Wei, T. Luo, *J. Phys. Chem. C* **2019**, *123*, 12659.
[125] V. Vishwakarma, C. Waghela, Z. Wei, R. Prasher, S. C. Nagpure, J. Li, F. Liu, C. Daniel, A. Jain, *J. Power Sources* **2015**, *300*, 123.
[126] J. L. He, L. Zhang, L. Liu, *Mater. Des.* **2020**, *194*, 108927.
[127] C. S. Tan, D. F. Lim, *ECS Trans.* **2013**, *50*, 115.
[128] J. Li, P. Agyakwa, C. Johnson, *Acta Mater.* **2010**, *58*, 3429.
[129] C. C. Li, C. K. Chung, W. L. Shih, C. R. Kao, *Metall. Mater. Trans. A* **2014**, *45a*, 2343.
[130] C. C. Yu, P. C. Su, S. J. Bai, T. H. Chuang, *Int. J. Precis. Eng. Manuf.* **2014**, *15*, 143.
[131] B.-S. Lee, S.-K. Hyun, J.-W. Yoon, *J. Mater. Sci.: Mater. Electron.* **2017**, *28*, 7827.
[132] W. Zhang, W. Ruythooren, *J. Electron. Mater.* **2008**, *37*, 1095.
[133] K. Bobzin, N. Bagcivan, L. Zhao, S. Ferrara, J. Perne, *Front. Mech. Eng.* **2010**, *5*, 370.
[134] Y. Tian, C. Hang, X. Zhao, B. Liu, N. Wang, C. Wang, *J. Mater. Sci.: Mater. Electron.* **2014**, *25*, 4170.
[135] J. Lu, K. Yuan, F. Sun, K. Zheng, Z. Zhang, J. Zhu, X. Wang, X. Zhang, Y. Zhuang, Y. Ma, X. Cao, J. Zhang, D. Tang, *ACS Appl. Mater. Interfaces* **2019**, *11*, 42708.
[136] F. Mu, Z. Cheng, J. Shi, S. Shin, B. Xu, J. Shiomi, S. Graham, T. Suga, *ACS Appl. Mater. Interfaces* **2019**, *11*, 33428.
[137] Y. Guo, Y. Zhou, Y. Xu, *Polymer* **2021**, *233*, 124168.
[138] A. Shanker, C. Li, G. H. Kim, D. Gidley, K. P. Pipe, J. Kim, *Sci. Adv.* **2017**, *3*, e1700342.
[139] G. J. Hu, B. Y. Cao, *J. Appl. Phys.* **2013**, *114*, 224308.
[140] X. Xu, J. Chen, J. Zhou, B. Li, *Adv. Mater.* **2018**, *30*, 1705544.
[141] A. K. Roy, B. L. Farmer, V. Varshney, S. Sihn, J. Lee, S. Ganguli, *ACS Appl. Mater. Interfaces* **2012**, *4*, 545.
[142] T. Zhang, T. F. Luo, *J. Phys. Chem. B* **2016**, *120*, 803.
[143] G. H. Kim, D. Lee, A. Shanker, L. Shao, M. S. Kwon, D. Gidley, J. Kim, K. P. Pipe, *Nat. Mater.* **2015**, *14*, 295.
[144] N. Song, D. L. Cao, X. Luo, Q. Wang, P. Ding, L. Y. Shi, *Composites, Part A* **2020**, *135*, 105912.
[145] D. An, X. Y. Duan, S. S. Cheng, Z. Y. Zhang, B. Yang, Q. S. Lian, J. X. Li, Z. J. Sun, Y. Q. Liu, C. P. Wong, *Composites, Part A* **2020**, *135*, 105928.
[146] F. H. Yang, X. P. Sun, X. Zhang, Z. H. Yao, *Appl. Surf. Sci.* **2021**, *569*, 151094.
[147] D. An, S. S. Cheng, S. Xi, Z. Y. Zhang, X. Y. Duan, Y. J. Ren, J. X. Li, Z. J. Sun, Y. Q. Liu, C. P. Wong, *Chem. Eng. J.* **2020**, *383*, 123151.
[148] P. B. Allen, J. L. Feldman, J. Fabian, F. Wooten, *Philos. Mag. B* **1999**, *79*, 1715.
[149] M. Simoncelli, N. Marzari, F. Mauri, *Nat. Phys.* **2019**, *15*, 809.
[150] L. Yang, B.-Y. Cao, *J. Phys. D: Appl. Phys.* **2021**, *54*, 505302.
[151] P. B. Allen, J. L. Feldman, *Phys. Rev. B* **1993**, *48*, 12581.
[152] L. Isaeva, G. Barbalinardo, D. Donadio, S. Baroni, *Nat. Commun.* **2019**, *10*, 3853.
[153] B. Sun, S. Niu, R. P. Hermann, J. Moon, N. Shulumba, K. Page, B. Zhao, A. S. Thind, K. Mahalingam, J. Milam-Guerrero, *Nat. Commun.* **2020**, *11*, 3810.
[154] Z. Feng, Q. Yu, S. Yao, L. Luo, W. Zhou, X. Mao, J. Li, J. Duan, Z. Yan, M. Yang, *Nat. Commun.* **2020**, *11*, 4968.
[155] S. Shenogin, A. Bodapati, P. Keblinski, A. J. McGaughey, *J. Appl. Phys.* **2009**, *105*, 034906.
[156] K. Aryana, D. A. Stewart, J. T. Gaskins, J. Nag, J. C. Read, D. H. Olson, M. K. Grobis, P. E. Hopkins, *Nat. Commun.* **2021**, *12*, 2817.
[157] Y. B. Liu, J. Y. Yang, G. M. Xin, L. H. Liu, G. Csányi, B. Y. Cao, *J. Chem. Phys.* **2020**, *153*, 144501.
[158] A. van Roekeghem, J. Carrete, C. Oses, S. Curtarolo, N. Mingo, *Phys. Rev. X* **2016**, *6*, 041061.
[159] S. Fujii, T. Yokoi, C. A. Fisher, H. Moriwake, M. Yoshiya, *Nat. Commun.* **2020**, *11*, 1854.
[160] H. Zhang, K. Hippalgaonkar, T. Buonassisi, O. M. L. LÃ¸vvik, E. Sagvolden, D. Ding, *ES Energy Environ.* **2018**, *2*, 1.
[161] Y. Liu, W. Hong, B. Cao, *Adv. Theory Simul.* **2022**, 2200037, https://doi.org/10.1002/adts.202200037.

Xu-Dong Zhang received his B.S. degree (2016) from Beijing University of science and technology, and Ph.D. degree (2021) in engineering thermophysics from Technical Institute of Physics and Chemistry, Chinese Academy of Sciences. Now, he works at Key Laboratory for Thermal Science and Power Engineering of Ministry of Education, Tsinghua University, as an assistant researcher. He works in the areas of liquid metal heat transfer, interfacial thermal transport, advanced electronic cooling, and electromagnetic fluid dynamics. He is a recipient of numerous awards like President Award of Chinese Academy of Sciences, and Excellent Paper of the Year Award from Frontiers in Energy.

Guang Yang received his B.S. degree in Energy and Power Engineering (2018) from Shandong University. Now, he is finishing Ph.D. degree under the supervision of Prof. Bing-Yang Cao in Engineering Thermophysics Program at Key Laboratory for Thermal Science and Power Engineering of Ministry of Education, Tsinghua University. His research focuses on interfacial thermal transport, micro-/nanoscale electronic thermal design, and thermophysical properties high-precision measurement. He is a recipient of numerous awards like "Yuzhi" Award for research on thermal properties measurement under Extreme Conditions.

Bing-Yang Cao is a professor in Department of Engineering Mechanics, Tsinghua University, China. He serves as chair of the Young Scientist Committee of the Heat and Mass Transfer Society of China, vice-chair of the Thermally Conductive Composite Committee of the Composite Society of China, executive committee member of the Asian Union of Thermal Science and Engineering etc. His main research areas include micro-/nanoscale heat transport, thermal functional materials and advanced thermal management technologies. He is Editor-in-Chief of ES Energy & Environment, and editorial member of nine international journals, including Journal of Physics: Condensed Matter, Scientific Reports, Materials etc.